Element abundances in the stars of the MILES spectral library: the Mg/Fe ratio

A. de C. Milone,[1,2]⋆ A. E. Sansom[2] and P. Sánchez-Blázquez[3]

[1]*Divisão de Astrofísica, Instituto Nacional de Pesquisas Espaciais, Av. dos Astronautas 1758, São José dos Campos, SP 12227-010, Brazil*
[2]*Jeremiah Horrocks Institute, University of Central Lancashire, Preston PR1 2HE*
[3]*Departamento de Fisica Teorica, Universidad Autónoma de Madrid, Cantoblanco 28049, Madrid, Spain*

ABSTRACT

We have obtained [Mg/Fe] measurements for 76.3 per cent of the stars in the Mid-resolution Isaac Newton Telescope Library of Empirical Spectra (MILES) spectral library used for understanding stellar atmospheres and stellar populations in galaxies and star clusters. These abundance ratios were obtained through (1) a compilation of values from the literature using abundances from high-resolution (HR) spectroscopic studies and (2) a robust spectroscopic analysis using the MILES mid-resolution (MR) optical spectra. All the [Mg/Fe] values were carefully calibrated to a single uniform scale, by using an extensive control sample with results from HR spectra. The small average uncertainties in the calibrated [Mg/Fe] values [respectively 0.09 and 0.12 dex with methods (1) and (2)] and the good coverage of the stars with [Mg/Fe] over stellar atmospheric parameter space of the library will permit the building of new simple stellar populations (SSPs) with empirical α-enhancements. These will be available for a range of [Mg/Fe], including both sub-solar and super-solar values, and for several metallicities and ages. These models will open up new prospects for testing and applications of evolutionary stellar population synthesis.

Key words: techniques: spectroscopic – astronomical data bases: miscellaneous – catalogues – stars: abundances – stars: atmospheres – solar neighbourhood.

1 INTRODUCTION

Evolutionary stellar population synthesis, i.e. modelling spectral energy distributions emitted by evolving stellar populations, is a natural approach to studying the stellar content of different galaxies. One of the main ingredients of these models is the stellar libraries, which can be empirical or theoretical. Stellar population models usually consider only the total metal content of stars and, therefore, ignore the different chemical abundance patterns that are present in individual stars. However, different chemical abundance patterns have a strong influence on the shape of the spectra. In particular, it is well known that stellar population models based on empirical libraries (which are mostly composed of solar neighbourhood stars) cannot reproduce the high values of Mg abundances found in giant elliptical galaxies. This is commonly interpreted as a consequence of high [Mg/Fe] in these systems, most likely due to a rapid star formation history compared to the more quiet one of the solar neighbourhood (Tinsley 1980).

An obvious solution, explored recently by several authors (e.g. Coelho et al. 2007; Walcher et al. 2009; Lee, Worthey & Dotter 2009), would be to use theoretical libraries with the desired coverage in chemical abundances. However, while theoretical libraries have

improved dramatically in the last few years (Chavez, Malagnini & Morossi 1997; Murphy & Meiksin 2004; Rodriguez-Merino et al. 2005; Munari et al. 2005; Martins et al. 2005; Coelho et al. 2005; Frémaux et al. 2006; Bertone et al. 2008), they still do not reproduce real stars of all spectral types, with especial problems depending on the wavelength range (i.e. Martins & Coelho 2007; Bertone et al. 2008). Some of the remaining problems are the incompleteness of the atomic and molecular line opacity lists in the blue region of the spectrum and for cool stars ($T_{\rm eff} < 4500$ K) as well.

Another approach is to compute, with the help of model atmospheres, response functions to characterize the variation of specific spectral characteristic (usually Lick indices) to variation of different elements (see Tripicco & Bell 1995; Korn, Maraston & Thomas 2005, hereafter K05). Models using these response functions are those of Tantalo, Chiosi & Bressan (1998), Trager et al. (2000a) and Thomas, Maraston & Bender (2003). However, the accuracy of these theoretical predictions has not been tested empirically yet.

It is the main objective of this work to provide [Mg/Fe] abundance ratios for one of the most complete empirical stellar libraries currently available, Mid-resolution Isaac Newton Telescope Library of Empirical Spectra (MILES; Sánchez-Blázquez et al. 2006). The MILES data base, which was especially designed for stellar population modelling, contains flux-calibrated optical spectra of high signal-to-noise ratio (S/N) for 985 stars covering $\lambda\lambda 3525$–7500 Å

⋆E-mail: acmilone@das.inpe.br

with a homogeneous resolution $\Delta\lambda =$ full width at half-maximum (FWHM) $= 2.3$ Å. The parametric coverage of sample stars in the three-dimensional Hertzsprung–Russell (H-R) diagram is quite wide: $2800 \leq T_{\rm eff} \leq 50\,400$ K, $0.0 \leq \log g \leq +5.0$ and $-2.7 \leq$ [Fe/H] $\leq +1.0$ dex, where [Fe/H] $= \log({\rm Fe/H})_\star - \log({\rm Fe/H})_\odot$ such that formally $\log({\rm Fe}) = \log(n({\rm Fe})/n({\rm H})) + 12$, $\log({\rm H}) = 12$, and $n({\rm Fe})$ and $n({\rm H})$ are the numerical densities (cm^{-3}) of iron and hydrogen atoms, respectively. The scales for these photospheric parameters were carefully defined by Cenarro et al. (2007). Their precisions, respectively, ±100 K, ±0.2 and ±0.1 dex, make MILES good for simple stellar population (SSP) modelling. For the present work, we excluded those stars with uncertain or wrong atmospheric parameters (see Vazdekis et al. 2010 for details about how these stars were identified).

The MILES [Mg/Fe] catalogue presented here consists of two measurement sets. The first one is composed of measurements obtained from the literature from high spectral resolution analyses properly calibrated to a common system. The second set assembles abundances measured by us directly from the MILES mid-resolution (MR) spectra and calibrated using the HR sample. The catalogue is represented in two separate tables for field and cluster stars. Both tables are available in full with the online version of the article (see Supporting Information). The paper layout is as follows. Section 2 describes the compilation of HR abundance measurements from the literature and their calibration; Section 3 shows the Mg abundance measurements from the MILES spectra; Section 4 compiles the MILES [Mg/Fe] catalogue and analyses its coverage over the library parameter space; Section 5 compares our stellar data with predictions of theoretical models focusing on the behaviour of some Lick indices with [Mg/Fe] and, finally, Section 6 plans for applications to building new SSP models with variable α-enhancement. Section 7 summarizes the whole paper and final conclusions. There are also three appendices: Appendix A confronts the compiled HR data with a well-known stellar spectrum library, Appendix B presents comparisons of the MILES photospheric parameter scales with those from the compiled HR studies and Appendix C compares the results for cluster stars with HR studies.

2 COMPILATION OF MAGNESIUM ABUNDANCES FROM HIGH-RESOLUTION STUDIES

The first step of this work consisted of performing a bibliographic compilation of magnesium abundances from HR spectroscopic analyses for the MILES library stars. To guarantee homogeneity between the measurements provided by several studies we performed a calibration and correction of systematic differences among sources and a chosen standard reference system, following a similar procedure as in Cenarro et al. (2001, 2007). For instance, Feltzing & Gustafsson (1998) give a detailed error analysis of elemental abundances for G and K metal-rich dwarfs also including comparisons with other studies. In this section, we describe the chosen reference sample and the procedures we followed to homogenize the measurements to a single uniform scale of [Mg/Fe].

2.1 A reference scale for [Mg/Fe]

Our reference sample to define a scale for the Mg/Fe abundance ratio is from Borkova & Marsakov (2005, hereafter BM05). The catalogue of Borkova & Marsakov is a robust compilation of the atmospheric parameters $T_{\rm eff}$, $\log g$ and [Fe/H] plus [Mg/Fe] from high S/N HR analyses of field stars published between 1989 and

2003 (covering 36 studies with Mg abundance determinations for around 900 stars). BM05 computed weighted average values and their errors through an iterative procedure in order to correct for the systematic deviations of each data set relative to reduced mean homogeneous scales. The uncertainty of [Mg/Fe] in BM05 is 0.05 and 0.07 dex, respectively, for metal-rich ([Fe/H] > -1.0 dex) and metal-poor stars ([Fe/H] ≤ -1.0 dex). The BM05 catalogue contains 218 stars in common with the MILES library (all with $\log g \geq 3.0$).

BM05 was also the reference work adopted in Cenarro et al. (2009), where Mg and Ca abundances were compiled for 192 stars of their calcium triplet stellar library (hereafter CaT) of 706 objects. As there are many MILES stars in common with the CaT sample (132 stars), this work provides values that we can compare with (see Appendix A).

2.2 Calibration of the high-resolution [Mg/Fe]

We first checked the possible presence of systematic differences in the scales of MILES and BM05 atmospheric parameters ([Fe/H], $\log g$ and $T_{\rm eff}$), however we did not find any (see Appendix B for details). Apart from the BM05 compilation, we obtained [Mg/Fe] for 97 more stars from 15 other HR studies, as listed in Table 1. Their abundance ratios were then carefully transformed on to the adopted scale as described next.

Fig. 1 shows the comparison of [Mg/Fe] for the stars in common between BM05 and other HR works. As can be seen, the relations are usually well described by an offset or a linear transformation. We derive these linear transformations using a 3σ clipping least-square (LSQ) method minimizing the distance in both axis (as the uncertainties in different studies are of comparable order).

$$[{\rm Mg/Fe}]_{\rm work} = A + B[{\rm Mg/Fe}]_{\rm BM05}, \tag{1}$$

where [Mg/Fe]$_{\rm work}$ represents the values computed in those HR works different from BM05. In BM05 and Cenarro et al. (2007), the comparison sample was gradually increased as each set of stellar parameters, like [Fe/H], was calibrated to a uniform scale. We, however, calibrate the [Mg/Fe] values separately for each work, basically because the comparison sample adopted here is large enough (218 stars from the BM05 compilation) and because this avoids the error propagation through the transformations. The calibrated values are obtained, then, inverting equation (1) as follows:

$$[{\rm Mg/Fe}]_{\rm HR} = (-A/B) + (1/B)[{\rm Mg/Fe}]_{\rm work}. \tag{2}$$

The transformation was performed only when A and B were significantly different from 0 and 1, respectively, based on the Student's t-test with a 95 per cent confidence level.

Table 1 presents the list of works and the number of stars in common between each sample and the BM05 catalogue, as well as the number of MILES stars to be included into our catalogue from each HR study and the number of MILES stars of each work duplicated in other source(s), whose total is 16. The calibration constants and the typical work uncertainties of [Fe/H] and [Mg/Fe] are shown in this table. We also show the [Fe/H] and [Mg/Fe] ranges of the stars included from these works. Comments about the local thermodynamic equilibrium (LTE) assumptions and spectral lines employed in each work are given in the table too. Statistically reliable linear calibrations of [Mg/Fe] were applied for the first nine works listed in Table 1. The data from Carretta et al. (2000), Fulbright (2000), Bensby et al. (2005), Erspamer & North (2003) and Feltzing & Gustafsson (1998) were not altered because there

Table 1. Parameters of the linear calibrations of different sets of [Mg/Fe] to the BM05 scale and other information about the consulted HR spectroscopic works. References are shown in the first column as: CGS00 (Carretta, Gratton & Sneden 2000), F00 (Fulbright 2000), Ge03 (Gratton et al. 2003), Be05 (Bensby et al. 2005), T98 (Thévenin 1998), RLA06 (Reddy, Lambert & Allende Prieto 2006), LH05 (Luck & Heiter 2005), EN03 (Erspamer & North 2003), FG98 (Feltzing & Gustafsson 1998), Ce02 (Caliskan et al. 2002), FK99 (Fulbright & Kraft 1999), H02 (Heiter 2002), Ae01 (Adelman et al. 2001), Ae06 (Adelman et al. 2006) and Ce09 (Cenarro et al. 2009). The $-A/B$ and $1/B$ values (second and third columns) are, respectively, the additive and multiplicative coefficients of the calibration expressions (equation 2). When they are represented by integer numbers it means that no calibration of [Mg/Fe] was applied because there are too few stars or none in common between the corresponding work and BM05 samples to compute a linear fit. N_c (forth column) represents the number of stars in common between each work and BM05 after applying the excluding criterion to each LSQ fit. N_i (fifth column) is the number of stars from each reference that are eligible to be included into the MILES [Mg/Fe] catalogue. N_r (sixth column) gives the number of MILES stars that are repeated in other works (once in each case). The [Fe/H] range of the stars to be included into our catalogue is shown in the seventh column and their [Mg/Fe] ranges (from the original values) are shown in the ninth column. The [Fe/H] and [Mg/Fe] intervals of the work samples in common with, respectively, the MILES and BM05 catalogues can be read in the plots of Figs 1 and A1. The typical uncertainties of [Fe/H] and [Mg/Fe] for each work are presented, respectively, in the eighth and tenth columns. In the eleventh column, the main physical constrains on measuring the Mg abundances are cited (LTE, non-LTE and the ionization stage of the Mg lines used in the abundance determination). The propagated uncertainty of [Mg/Fe] over the calibration process for each data sample is written in the last column. The weighted averages of [Mg/Fe] errors are given in the eleventh row for 103 stars whose data come from the first nine works. The weighted averages of [Mg/Fe] errors for nine stars of the five last listed works (that do not have stars repeated in other works nor were their data calibrated to the [Mg/Fe] uniform scale in the current work) are shown in the penultimate row.

Ref.	$-A/B$ (dex)	$1/B$	N_c	N_i	N_r	$[\text{Fe/H}]^i_{l,u}$ (dex)	$\delta[\text{Fe/H}]$ (dex)	$[\text{Mg/Fe}]^i_{l,u}$ (dex)	$\delta[\text{Mg/Fe}]$ (dex)	Notes	$\sigma[\text{Mg/Fe}]$ (dex)
CGS00	0.000	1.000	9	5	3	$-2.63, +0.13$	0.08	$+0.04, +0.64$	0.09	non-LTE, Mg I	0.09
F00	0.000	1.000	20	18	7	$-2.64, -0.99$	0.04	$+0.25, +0.61$	0.07	LTE, Mg I	0.07
Ge03	-0.076	0.997	132	2	1	$-1.49, -0.75$	0.05	$+0.19, +0.63$	0.09	LTE, Mg I	0.09
Be05	0.000	1.000	84	1	1	-0.75	0.10	$+0.42$	0.06	LTE, Mg I	0.06
T98	0.029	0.974	224	44	9	$-2.63, +0.60$	<0.20	$-0.58, +0.80$	<0.20	LTE, Mg I	0.20
RLA06	-0.065	1.392	59	1	1	-1.01	0.08	$+0.35$	0.05	LTE, Mg I	0.07
LH05	-0.103	1.000	56	16	5	$-0.60, +0.16$	0.06	$-0.02, +0.57$	0.13	LTE, Mg I	0.13
EN03	0.000	1.000	7	10	3	$-1.19, +0.28$	0.18	$-0.34, +0.17$	0.10	LTE, Mg I	0.18
FG98	0.000	1.000	7	6	1	$+0.02, +0.26$	0.18	$-0.06, +0.18$	0.13	LTE, Mg I	0.13
				103	31				$<0.15>$		$<0.17>$
Ce02	0	1	2	1	1	0.00	0.20	0.00	0.21	LTE, Mg I	0.21
				104	32						
				-16							
Sum				88							
FK99	0	1	1	1	0	-2.55	0.06	$+0.60$	0.09	LTE, Mg I	0.09
H02	0	1	0	1	0	-1.02	0.10	$+0.32$	0.10	LTE, Mg I, Mg II	0.10
Ae01	0	1	0	3	0	$-0.56, +0.20$	0.16	$+0.02, +0.20$	0.16	LTE, Mg I, Mg II	0.16
Ae06	0	1	0	1	0	-0.74	0.14	$+0.28$	0.14	LTE, Mg II	0.14
Ce09	0	1	0	3	0	$-2.59, -1.73$	0.10	$+0.27, +0.47$	0.14	LTE, Mg I	0.14
Sum				9					$<0.14>$		$<0.14>$
Total				97							

is no detectable difference between the [Mg/Fe] scales of these works and the BM05 scale. No calibration was applied, either, to the data from the six last entries of Table 1: Caliskan et al. (2002) and Fulbright & Kraft (1999), because there are very few stars in common with the BM05 sample; Heiter (2002) and Adelman et al. (2001, 2006) because there is no star in common; and Cenarro et al. (2009) because their data are already on the same system we have adopted too (see Appendix A).

16 stars have [Mg/Fe] values from duplicated sources. When the difference between distinct sources is larger than 4σ, then the values with smaller uncertainties were adopted (three cases only). The final abundance ratios for the 13 remaining duplicated cases were computed as simple averages after separately calibrating to the BM05 scale. These stars were also used to evaluate the calibration process as a whole and helped us to compare the uncertainties of [Mg/Fe] when there are duplicated or single data sources (see Section 2.3).

Summarizing, the [Mg/Fe] catalogue of MILES contains 315 stars with HR measurements (see Table 1):

(i) 218 stars with [Mg/Fe] collected directly from BM05,

(ii) 91 stars with [Mg/Fe] obtained from other published works and calibrated to the same single uniform scale and

(iii) six stars whose [Mg/Fe] ratios were collected from other works and inserted into it without any transformation.

2.3 Precision of calibrated [Mg/Fe]

The uncertainties of calibrated [Mg/Fe] to the BM05 scale were estimated through the propagation of their original errors taking also into account the precision of calibration parameters (see Table 1 and plots of Fig. 1). The error propagation through the linear expressions of calibration process was based on adding variances. The [Mg/Fe] uncertainties can be summarized as follows.

(i) 0.07 and 0.05 dex for the 218 stars that define the base uniform scale, for, respectively, [Fe/H] ≤ -1.0 dex (47 stars) and [Fe/H] > -1.0 dex (171 stars) (as described in BM05);

(ii) 0.17 dex for 75 stars (weighted average) whose abundance ratios were calibrated from single values;
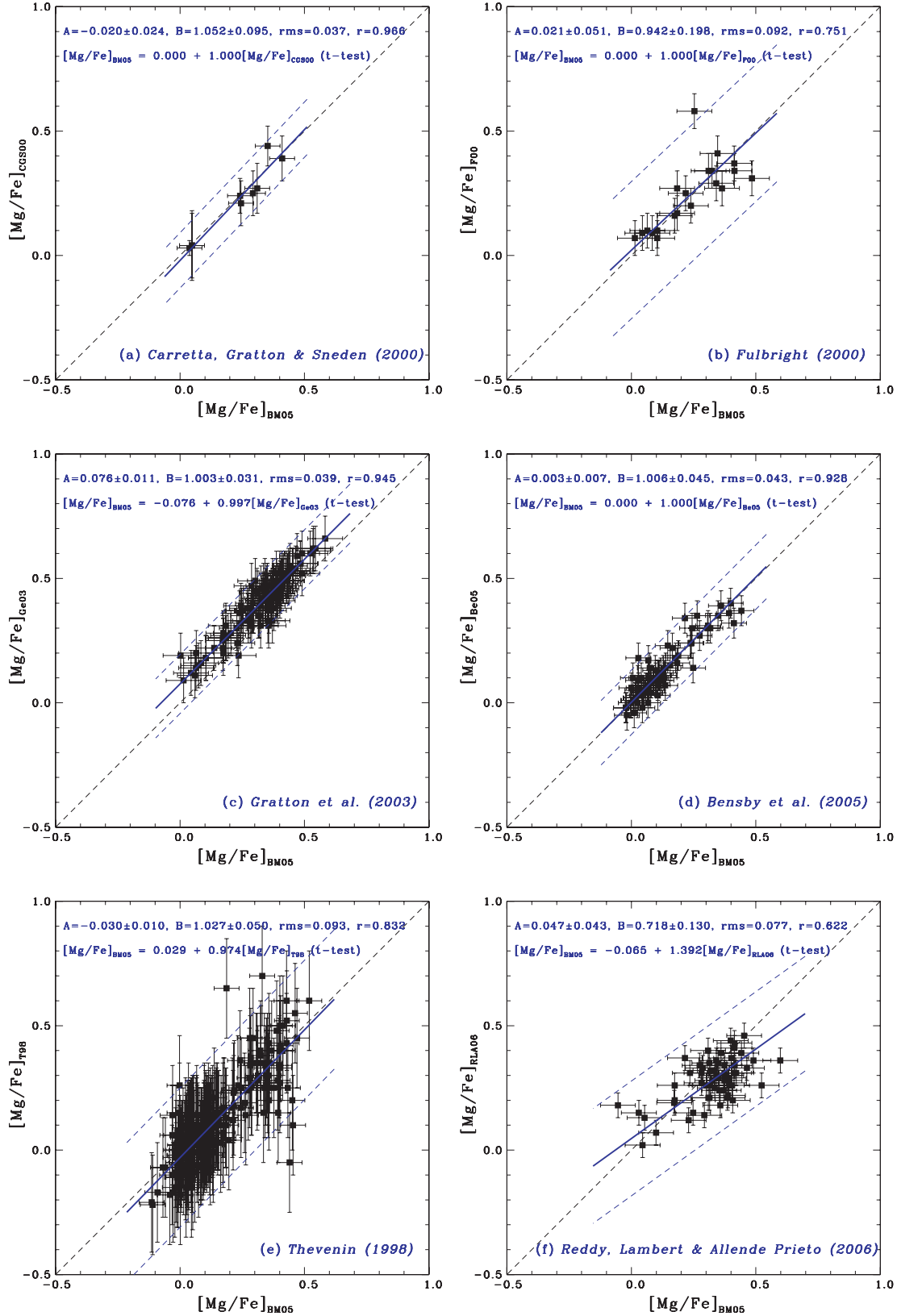
Figure 1. [Mg/Fe]$_{work}$ as a function of [Mg/Fe]$_{BM05}$: nine panels (a to i) showing comparisons between different samples with the reference set from BM05. The statistically representative, 3σ-clipped (illustrated by parallel dashed blue lines), linear LSQ fittings are presented by the thick blue lines (clipped data are represented by red symbols, occurring in the last panel only). The constants A and B and parameters *rms* and r (correlation coefficient) of the linear fits (equation 1) are listed at the top of each panel. The calibration expressions of [Mg/Fe]$_{work}$ to [Mg/Fe]$_{BM05}$ (equation 2) are also shown after applying the 95 per cent *t*-test. The work designation is cited at the bottom of each panel.
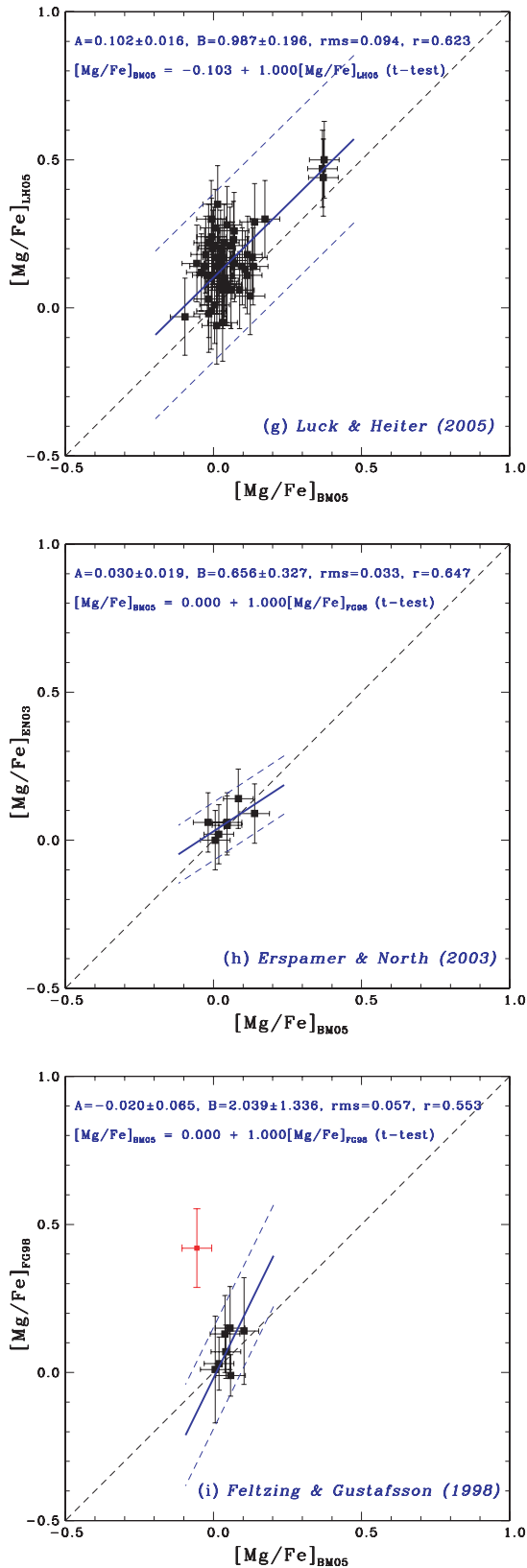
Figure 1 – *continued*

(iii) 0.10 dex for 13 stars based on average calibrated abundance ratios (data from duplicated sources);

(iv) 0.14 dex for three stars from Ce09;

(v) 0.13 dex for six other stars whose [Mg/Fe] were not transformed on to the BM05 scale.

The averaged [Mg/Fe] values compiled from duplicates are statistically more precise ($1\sigma = 0.10$ dex) than the calibrated abundance ratios that have been computed from single sources ($1\sigma = 0.17$ dex). The final weighted average uncertainty of [Mg/Fe] is around 0.09 dex over all compiled HR data (315 stars). It is 0.10 dex for 88 metal-poor stars ([Fe/H] ≤ -1.0 dex) and 0.08 dex for 227 metal-rich ones ([Fe/H] > -1.0 dex). The mean uncertainty of [Mg/H] over whole range of metallicity is 0.13 dex, estimated by the quadratic sum of σ[Fe/H] and σ[Mg/Fe].

2.4 Extended control sample for calibrating [Mg/Fe]

In total, we compiled [Mg/Fe] for 315 MILES stars covering about 1/3 of the library (263 dwarfs and 52 giants, respectively 49 per cent and 12 per cent of them), which was used to define an extensive control sample for calibrating our own Mg abundance measurements at MR (Section 3). Dwarfs as designated when log $g \geq 3.0$ whilst giants when log $g < 3.0$, as in BM05 and the MILES data base itself.

Fig. 2 shows [Mg/Fe] versus [Fe/H] for the HR part of the MILES [Mg/Fe] catalogue and its parametric coverage is shown in Table 6 (Section 4). Specifically, the control sample owns 306 stars covering nearly 31 per cent of MILES (255 dwarfs and 51 giants) and practically presenting the same coverage. Besides six stars whose [Mg/Fe] has not been transformed on to the reference scale, three chemically peculiar metal-poor stars (BD+800245 confirmed by Ivans et al. 2003, HD 097855, and HD 192640) have also been excluded from the control sample because their [Mg/Fe] lay far from the [Mg/Fe] versus [Fe/H] trend described by the stars in the solar neighbourhood (see Fig. 2). Recently, Nissen & Schuster (2010) have classified Galactic objects as low-α-enhancement stars distributed over two distinct nearby halo populations based on their kinematics, whose origins might be due to the accretion from dwarf galaxies and some of them from the Omega Centauri globular cluster (denominated as a progenitor galaxy). HD 097855 might belong to the proposed group. All of those nine stars have been incorporated into our catalogue.

3 MAGNESIUM ABUNDANCES MEASURED AT MID-RESOLUTION

To extend the magnesium abundance characterization of the MILES stars, a spectroscopic analysis based on an LTE spectral synthesis of Mg features was carried out at MR.

Recovering element abundances in stellar photospheres at medium spectral resolution (resolving power between 1000 and 10 000) has been a well-established and alternative approach for many decades. For instance, Pagel (1970) reported that low-resolution spectroscopic analysis was one way to find the metallicity of nearby stars, by calibrating the results with a reference sample which, indeed, has been highlighted as an important step involved (Friel & Janes 1993; Kirby et al. 2009; Marsteller et al. 2009).

Our present Mg abundances reported in the current section of the paper are based on the MILES spectra, which have a resolution comparable to many previous studies (e.g. Chavez, Malagnini & Morossi 1995; Terndrup, Sadler & Rich 1995; Cook et al. 2007).
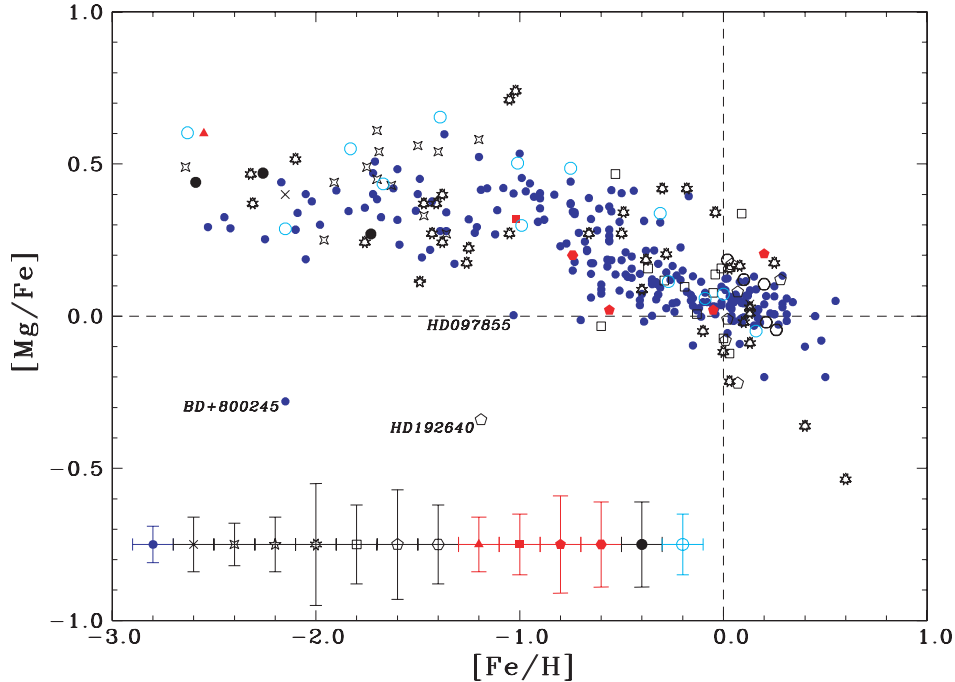
Figure 2. [Mg/Fe] versus [Fe/H] for the HR data of MILES [Mg/Fe] catalogue (summing 315 stars). [Fe/H] is on the MILES scale (Cenarro et al. 2007). The sources are represented by different symbols: BM05 catalogue as filled blue circles (218 stars), CGS00 as diagonal crosses (two objects), F00 as four-pointed stars (13 objects), Ge03 as five-pointed stars (one object), T98 as eight-pointed stars (35 objects), LH05 as open squares (12 objects), EN03 as open pentagons (seven objects), FG98 as open hexagons (five objects), FK99 as filled red triangles (one object), H02 as filled red squares (one object), Ae01 as filled red pentagons (three objects), Ae06 as filled red hexagons (one object) and Ce09 as filled black circles (three objects). The data for 13 stars, whose sources are duplicated, are represented by open cyan circles. The red symbols represent stars whose [Mg/Fe] were not calibrated to the uniform scale (six cases). The designations of works are cited in the caption of Table 1. Three chemically peculiar stars are identified by their names.

3.1 Computation of the synthetic spectra

Our analysis is based on an LTE spectral synthesis computed with the most recent stable version of the MOOG code at the time of developing this work (Sneden 2002). The synthesis code was fed by linearly interpolated model atmospheres over the MARCS 2008 grid (Gustafsson et al. 2008), up-to-date atomic line lists from the Vienna Atomic Line Data base (VALD; Piskunov et al. 1995; Ryabchikova et al. 1997; Kupka et al. 1999, 2000) and a set of important molecular lines of C_2, CN and MgH (Kurucz 1995) in order to compute a series of model spectra for each MILES star ranging over five values of [α/Fe]: −0.60, −0.30, 0.00, +0.30, +0.60 dex.

The abundance of all α-particle-capture elements – O, Ne, Mg, Si, S, Ar, Ca and Ti – was equally and simultaneously modified to represent a global variation of their chemistry in a stellar photosphere. Although these elements may have distinct individual abundance ratios relative to iron, assuming homogeneity for them should be a reliable approximation among many computations such as molecular dissociative equilibrium and partial pressure of different species, especially when the element abundances are not individually and previously known in each star. Moreover, globally changing these ratios for all α-elements is coherent with the model atmospheres adopted in our spectral synthesis. We tested the alternative approach at medium spectral resolution (i.e. varying the Mg abundance only, keeping the abundances of other α-elements fixed) for some MILES stars and the effect was negligible. Even adopting the homogeneous global trend for the α-elements, their individual abundances can be independently measured by separately analysing their own absorption features. For instance, the Mg abundance is only consistently quantified as one or more magnesium lines are

analysed instead of computing and measuring features of other α-elements.

We selected model atmospheres whose chemistry follows the general pattern of solar neighbourhood for the α-elements (the standard composition group of the MARCS 2008 models; Gustafsson et al. 2008), i.e. [α/Fe] = +0.40 dex when [Fe/H] ≤ −1.00 dex and [α/Fe] = 0.00 dex for [Fe/H] ≥ 0.00 dex with intermediate variable values between these fiducial metallicities (+0.30, +0.20 and +0.10 dex for [Fe/H] = −0.75, −0.50 and −0.25 dex, respectively). On this standard range of compositions, every other element (X) follows the iron abundance, [X/H] = [Fe/H] meaning [X/Fe] = 0 dex. An MARCS model presents a stratification over 56 plane-parallel layers for its photosphere. In the case of giants, the models (with −0.5 ≤ log g ≤ 3.5 in the MARCS grid) have been originally generated under a three-dimensional geometry for different masses and afterwards transformed on to one-dimensional representations by their own developers. We chose 3D models with one solar mass for giants (log g < 3.0 in the current work). All chosen models for dwarfs (with 3.0 ≤ log g ≤ 5.5 in the grid) and giants have a microturbulence velocity of 2.0 km s^{-1}. The MARCS 2008 grid ranges are as follows.

(i) 2500 ≤ T_{eff} ≤ 8000 K with steps of 100 K for T_{eff} < 4000 K and 250 K for T_{eff} ≥ 4000 K;

(ii) −1.0 ≤ log g ≤ 5.0 (or 5.5 in some cases) with 0.5 constant steps;

(iii) [Fe/H] = −5.00, −4.00, −3.00, −2.00, −1.50, −1.00, −0.75, −0.50, −0.25, 0.00, +0.25, +0.50, +0.75 and +1.00 dex.

Linear interpolations of the model atmospheres were automatically done by using the user-friendly software of Masseron (2008),

which is publicly available from the MARCS models' web-site (http://marcs.astro.uu.se/). The layers of each input model to the MOOG code were represented by the optical depth at 5000 Å, the thermodynamic equilibrium temperature, the total gas pressure and the electron numeric density (all quantities in cgs units). The microturbulence velocity was fixed at $2.0\,km\,s^{-1}$ for all layers of each model. The effective broadening is dominated by the spectroscopic instrumentation and is suitably represented by a Gaussian convolution.

Our spectral synthesis computations adopt the same solar abundance pattern used to build up the MARCS 2008 model atmospheres (Grevesse, Asplund & Sauval 2007, hereafter GAS07), aiming at an important internal consistency regarding the reference solar chemistry. The solar abundances in GAS07 of those α-elements on a logarithm scale are: $\log(O) = 8.66$, $\log(Ne) = 7.84$, $\log(Mg) = 7.53$, $\log(Si) = 7.51$, $\log(S) = 7.14$, $\log(Ar) = 6.18$, $\log(Ca) = 6.31$ and $\log(Ti) = 4.90$. The abundance of iron is given by $\log(Fe) = 7.45$ on this scale.

Many authors re-scale the oscillator strengths (gf) of atomic lines to reproduce the solar spectrum, i.e. calibrate the line strengths to the Sun's photospheric conditions. However, we preferred to maintain their laboratory gf values from VALD instead of normalizing them to the solar scale because we intend to calibrate our MR measurements using our HR control sample. The theoretical spectra were calculated at 0.02 Å wavelength steps by assuming an opacity contribution for the stellar continuum at 0.50 Å bins. For the often strong Mgb lines (see Section 3.2 and Table 2), we adopted the Unsöld approximation for the interaction constant (C_6) of the van der Waals dump parameter γ_6 multiplied by a 6.3 factor. This dumping represents collisions among neutral atomic species mainly H I and He I as in cold photospheric layers. On the other hand, the same constant multiplied by an MOOG internal factor was chosen for the other Mg feature. The Unsöld approximation (default in MOOG) means that C_6 is basically due to the H I atoms as a function of the excitation potential of an electronic transition, but γ_6 remains also dependent on the local gas pressure and temperature.

All our model spectra were computed at the MILES resolution, which is slightly different in each Mg feature region (FWHM = $\Delta\lambda$ = 2.40 Å for Mg5183 and 2.35 Å for Mg5528), by applying Gaussian smoothing to represent the (instrumental dominated) broadening. At this resolution, no additional stellar rotational broadening needs to be considered unless the line-of-sight rotational velocity $v_{rot}\sin(i)$ is greater than $\sim$130 km s^{-1}. The wavelength scales of all MILES observed spectra were carefully shifted to the rest wavelength to match the theoretical model scales, i.e. wavelengths in air as available in the VALD data base for λ from 2000 Å up to the infrared. Spectral cross-correlations were applied for this purpose through the cross-correlation FXCOR task of the Radial Velocity Analysis Package of the NOAO Optical Astronomy Pack-

ages of IRAF (Image Reduction and Analysis Facility)[1] by adopting a given correspondent model spectrum for each star as a template. The model spectra computed for either [Mg/Fe] = +0.60 or +0.30 dex were chosen in order to guarantee reliable spectroscopic cross-correlations for all MILES spectra, from the hottest metal-poor to the coldest metal-rich ones, i.e. with strong absorption lines in the template spectra. Then the wavelength scales of all computed spectra were re-binned to exactly agree with the sampling of the MILES spectra at each observed wavelength bin (0.90 Å). Finally, flux normalizations of the empirical spectra based on the local pseudo-continuum were carefully applied at the regions around each Mg feature in order to adequately match to the flux normalized scale of the theoretical spectra. Fiorentin et al. (2007) emphasized the importance of performing reliable comparisons on compatible flux and wavelength scales between observed MR spectra and synthetic ones, paying special attention to choosing useful absorption features and accurately calibrating the abundance results.

3.2 Mg features analysed: Mg5183 and Mg5528

Two strong Mg features were chosen and carefully tested to be measurable and useful for recovering magnesium abundances at the MILES spectral resolution with acceptable precision for generating new stellar population models with [Mg/Fe] constraints, i.e. with comparable precision to that of [Fe/H] in MILES (0.10 dex). These features are: (i) the reddest line of the Mgb triplet (λ5183.604 Å) named here Mg5183, which is usually the strongest and the most Mg sensitive of the three lines, and (ii) MgIλ5528.405 Å (hereafter Mg5528).

3.3 Methods applied: pseudo-equivalent width and line profile fit

Two methods were chosen to measure the magnesium abundances:

(i) based on pseudo-equivalent widths, hereafter EW (pseudo-ones in fact due to the extensive line blanketing at the MILES spectrum resolution), and

(ii) applying line profile fittings (LPF).

These methods are usually adopted on HR and MR analyses and both require a previous knowledge of the photospheric parameters. When there are more than two lines of an element, the modelling of their equivalent widths is preferable instead of fitting their profiles. The fit of line profiles is commonly adopted to extract element abundances from molecular absorptions where a myriad of lines from a single substance are very close to each other. When analysing atomic features, both methods generally need isolated lines; however, they can work on composite lines that can be de-blended in single profiles if the abundances of the other absorbers are already known. Traditionally, the EW method is applied in an automatic process to extensive sets of lines. On the other hand, the second method is employed focusing on careful visual inspection in a feature-by-feature and star-by-star base. The abundance precision derived from each method depends on how many features are adopted and how sensitive each absorption line is to a given elemental abundance variation.

Table 2. The magnesium features: their central pass-bands Feature$_{band}$ and two pseudo-continuum windows c_b and c_r, adopted for defining linear local continua for measuring their pseudo-equivalent widths.

Feature	c_b (Å)	Feature$_{band}$ (Å)	c_r (Å)
Mg5183	5177.4–5178.3	5179.2–5187.3	5199.9–5200.8
Mg5528	5518.0–5521.0	5524.0–5531.0	5539.0–5542.0

At each chosen Mg feature region, we automatically applied these methods as explained below.

(i) The equivalent width of a weak line is proportional to the number of absorbers of element X [EW $\propto n(X)$], whilst the equivalent widths of strong lines are dependent on $n(X)^{1/2}$. Therefore, direct comparisons were made on planes [Mg/Fe] versus log(EW) by adopting simple linear LSQ fittings for each set of theoretical equivalent widths. Note that the iron abundance [Fe/H] is fixed in all model computations for each star (like the other photospheric parameters assuming those compiled by Cenarro et al. 2007) and [Mg/Fe] = [Mg/H] − [Fe/H]. Therefore we adopt that relationship instead of the direct log(EW) versus log($n(X)$). Consequently, [Mg/Fe] can be directly measured instead of [Mg/H] and they were obtained through interpolation of the [Mg/Fe] versus log(EW) relationship for each star and feature combination. The equivalent width measurements of both Mg features were performed with the LECTOR code (A. Vazdekis' webpage, www.iac.es/galeria/vazdekis/SOFTWARE/) and INDEXF software (www.ucm.es/info/Astrof/software/indexf), however, the uncertainties have been estimated through INDEXF only. Both software provided the same results within an accuracy of milli-Angstroms. The measurements were carried out within the central passband of each Mg feature by adopting a linear local flux continuum that is defined by the average fluxes and wavelengths of two pseudo-continuum windows held very near to the passband (at each side of the feature). The central passband and pseudo-continuum windows of both Mg features were carefully chosen in order to provide representative measurements for their equivalent widths and are presented in Table 2. We computed the equivalent width uncertainties as being dominated by photon statistics based on the formalism from Cardiel et al. (1998). The relative uncertainties are distributed between few per cents and 40 per cent, whilst the equivalent widths range from 0.15 up to 2.60 Å and from 0.05 up to 0.95 Å for the Mg5183 and Mg5528 features, respectively. We noted that the EW uncertainties are dependent on the spectral S/N, as expected, and it is more evident for the Mg5183 feature. The higher S/N, smaller is the EW relative error. The S/N has been computed as an average between the blue and red regions of MILES stellar spectra, and it ranges from 10 up to 550 per Å with typical values around 235 per Å. It is also noted that there is a strong inverse correlation between the relative errors and the equivalent width values.

(ii) The line profile comparison between the observed Mg feature and each corresponding set of synthesized features was made within the central passband through *rms* statistics. Optimal [Mg/Fe] from each feature were derived for each MILES' star through *rms* minimization, as is shown in Fig. 3 for a dwarf and giant spectra. The pseudo-continuum windows were adopted to accurately match the continuum fluxes of the observed and model spectra. Careful attention was paid to specific cases for which the theoretical and observed spectra do not match each other simultaneously at both continuum windows. Minor corrections were applied to the observed spectrum continuum flux for this purpose based on eye-trained inspections (additive or multiplicative corrections). Each curve of *rms* as a function of [Mg/Fe] was fitted by a spline.

Fig. 3 shows examples of spectral synthesis of the Mg5183 and Mg5528 regions for a dwarf and giant. The main panels of each sub-figure (for each combination star-feature) present the MILES spectrum compared with model spectra. The sub-figures also include graphs illustrating the abundance measurement methods.

The global procedure for obtaining and calibrating [Mg/Fe] ratios from our MR spectra is as follows:

(i) automatic measurements at each Mg feature by applying both methods to obtain [Mg/Fe]$_{\mathrm{feature}}^{\mathrm{method}}$;

(ii) for each feature, computation of simple averages from the two methods when both show reliable results checked through visual inspections to get [Mg/Fe]$_{\mathrm{feature}}$ (in some cases, only one method results in a reliable value and in other cases, both methods fail);

(iii) linear calibration of [Mg/Fe]$_{\mathrm{feature}}$ to a uniform scale, separately for each feature, via comparison with the HR star control sample (described at Section 2.4), to compute [Mg/Fe]$_{\mathrm{feature}}^{\mathrm{calib}}$;

(iv) simple averaging of the calibrated ratios obtained from both features combined when possible, in order to obtain the final calibrated abundance ratios [Mg/Fe]$^{\mathrm{calib}}$.

When the spectral synthesis of a given Mg feature does not satisfactorily reproduce the observed stellar spectrum (equivalent width and/or absorption line profile), we call this a non-reproduced spectral synthesis and classify it such as (a) inadequate reproduction of the observed spectral continuum, (b) saturation effect on the [Mg/Fe] versus log(EW) relationship (non-linearity), (c) extrapolation on the [Mg/Fe] versus log(EW) relationship and/or on the rms_{LPF} versus [Mg/Fe] one, (d) possible inaccurate model atmosphere interpolation (i.e. done around the borders of the MARCS 2008 grid), (e) possible higher rotation velocity than 130 km s^{-1}, (f) absence of molecular lines to compute the model spectrum (e.g. TiO bands), (g) low-quality observed spectrum (S/N below 50 per Å), (h) possible wrong photospheric parameters, (i) suspect chemically peculiar star and (j) other unknown causes and effects. Consequently, the abundance ratio provided by the correspondent method is not reliable.

Calibration of each [Mg/Fe]$_{\mathrm{feature}}$ was applied after averaging the measurements obtained from both methods. We decided to compute simple averages because each method explores one aspect of a reliable spectral synthesis. Whilst the EW comparison focuses on the reproduction of the total energy absorbed by the feature relative to the local continuum, the line profile fit takes into account the line shape including the core and wings.

Moreover, the absolute differences between EW and LPF methods are always smaller than 3σ[Mg/Fe]$_{\mathrm{feature}}$ (around 0.03 dex for Mg5183 and 0.07 dex for Mg5528). We checked for dependences of the differences between methods on the atmospheric parameters T_{eff}, log g and [Fe/H] and the results do not show any dependence, for both features. We also noted there is no parametric dependence of the differences ([Mg/Fe]$_{\mathrm{feature}}^{\mathrm{EW}}$ − [Mg/Fe]$_{\mathrm{HR}}$) and ([Mg/Fe]$_{\mathrm{feature}}^{\mathrm{LPF}}$ − [Mg/Fe]$_{\mathrm{HR}}$) for both Mg features and methods.

3.4 Calibration of the mid-resolution [Mg/Fe]

The calibration to the previously adopted uniform scale relies on an inverse linear transformation,

$$[\mathrm{Mg/Fe}]_{\mathrm{feature}}^{\mathrm{calib}} = (-a/b) + (1/b)[\mathrm{Mg/Fe}]_{\mathrm{feature}} \qquad (3)$$

that is obtained through a 3σ clipping simple linear LSQ fit of our MR measurements as a function of the HR calibrated values from the [Mg/Fe]$_{\mathrm{HR}}$ star control sample (Section 2.4). We also applied a 95 per cent t-test to verify if the fit parameters a and b are distinguishable from zero and unity, respectively. In case they were not, we would adopt $a = 0$ and $b = 1$.

Fig. 4 shows the comparisons of [Mg/Fe]$_{\mathrm{Mg5183}}$ and [Mg/Fe]$_{\mathrm{Mg5528}}$ against [Mg/Fe]$_{\mathrm{HR}}$, in which the linear LSQ fittings are presented simultaneously for dwarfs and giants. The computed calibration expressions are

$$[\mathrm{Mg/Fe}]_{\mathrm{Mg5183}}^{\mathrm{calib}} = 0.058 \ \mathrm{dex} + 1.546[\mathrm{Mg/Fe}]_{\mathrm{Mg5183}} \qquad (4)$$
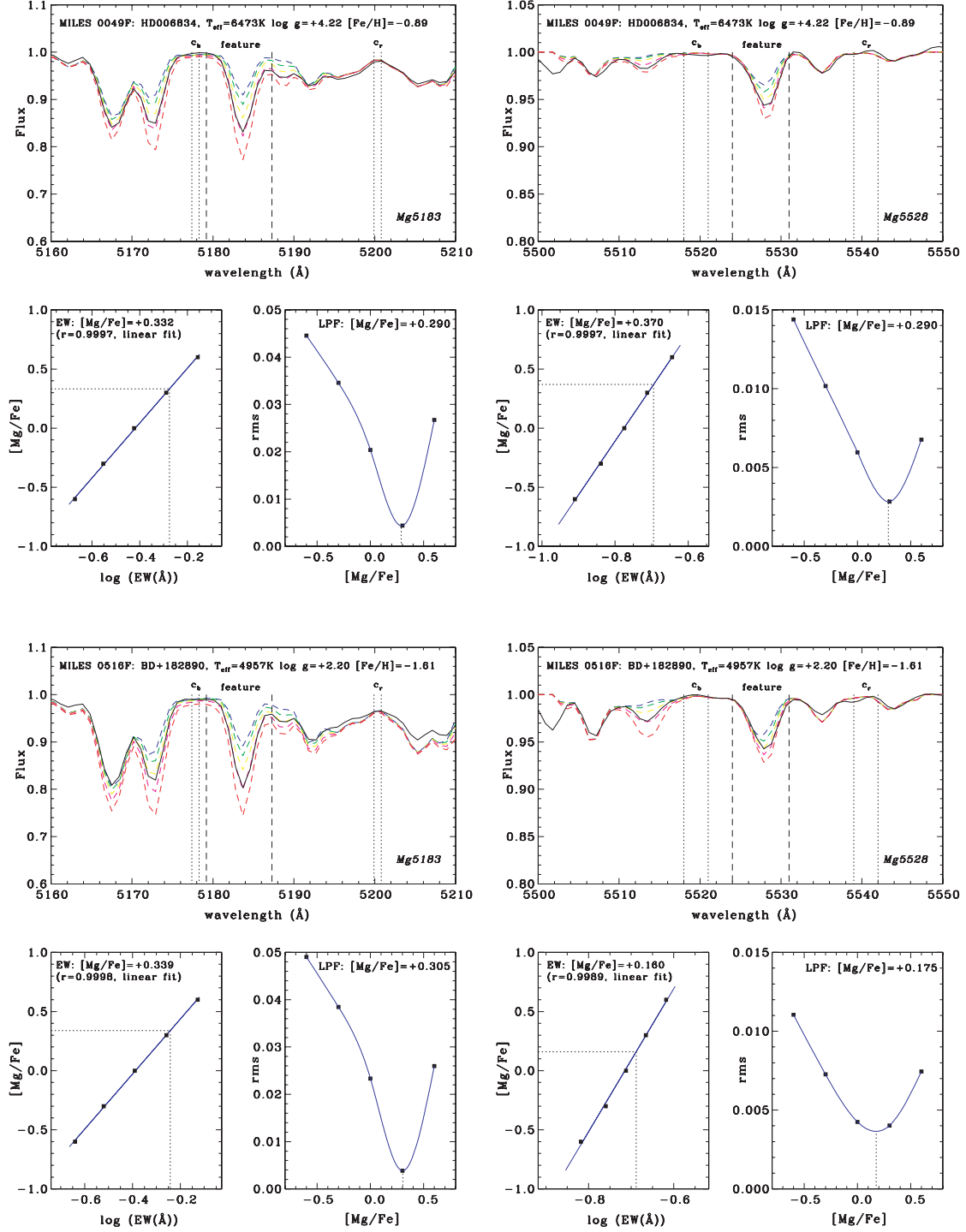
**Figure 3.** Examples of spectral synthesis of the Mg5183 and Mg5528 features for a MILES' dwarf (HD 006834: $T_{eff} = 6473$ K, $\log g = 4.22$, [Fe/H] = −0.89 dex, at the two top sub-figures) and giant (BD+182890: $T_{eff} = 4957$ K, $\log g = 2.20$, [Fe/H] = −1.61 dex, at the two bottom sub-figures). Their central bandpass and two pseudo-continuum windows, c_b and c_r, are shown in the main panel of each sub-figure. The observed spectrum is represented by the solid black line and the synthetic ones by the colour dashed lines. Each set of theoretical spectra was computed for five α-enhancements ([α/Fe] = −0.60, −0.30, 0.00, +0.30, +0.60 dex, respectively, on colours blue, green, yellow, magenta and red) assuming the star's photospheric conditions fixed. Two small graphs illustrate the two abundance determination methods in each sub-figure: EW (bottom-left corner) and LPF (bottom-right corner) presenting their [Mg/Fe]$_{feature}^{method}$.

$$[Mg/Fe]_{Mg5528}^{calib} = 0.227 \text{ dex} + 1.011[Mg/Fe]_{Mg5528}. \quad (5)$$

The calibrated abundance ratios [Mg/Fe]^{calib} from the Mg5183 and Mg5528 features that respectively lay outside the intervals [−0.42 dex, +0.92 dex] and [−0.41 dex, +0.88 dex] are based on extrap-

olations over the calibrations. The intervals were estimated taking into account the [Mg/Fe]$_{feature}$ scale coverages of the stellar common sample between the HR compilation data and our MR measurements as well as the internal uncertainties of [Mg/Fe]$_{Mg5183}$ and [Mg/Fe]$_{Mg5528}$ (described in Section 3.5). Therefore, the
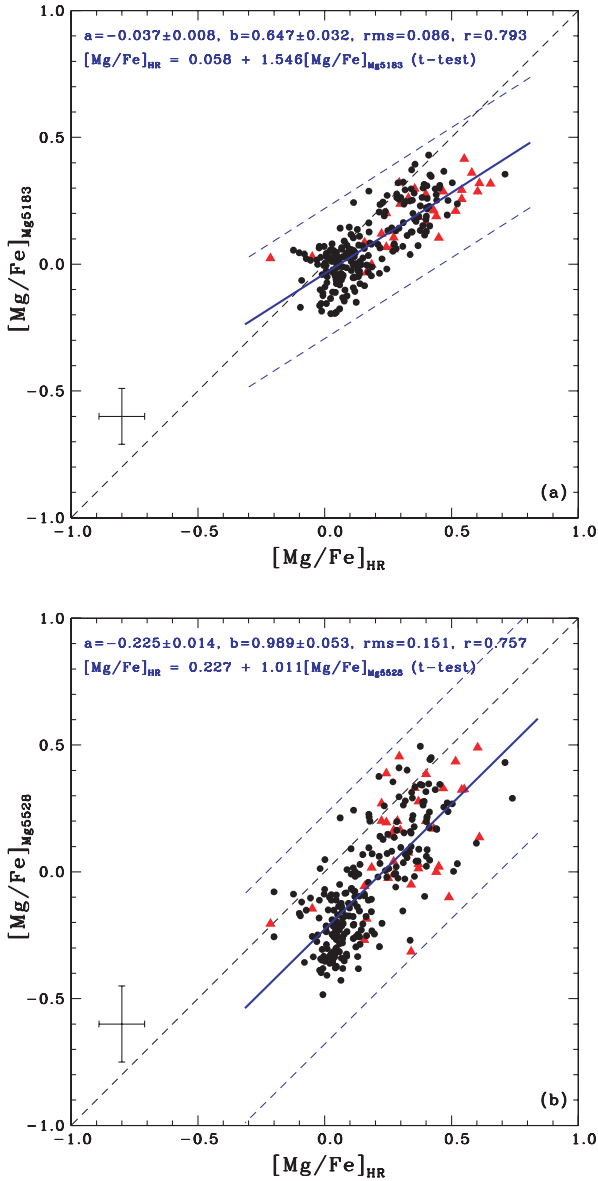
Figure 4. $[Mg/Fe]_{Mg5183}$ versus $[Mg/Fe]_{HR}$, top panel (a), and $[Mg/Fe]_{Mg5528}$ versus $[Mg/Fe]_{HR}$, bottom panel (b), comparisons for dwarfs and giants together in each, respectively represented by black filled circles and red filled triangles. The straight line inversely derived from the simple linear LSQ fit $[Mg/Fe]_{feature} = a + b[Mg/Fe]_{HR}$ is also shown for each comparison (blue solid line) with two parallel blue dashed lines illustrating the 3σ clipping procedure. The parameters a and b are displayed on the top of graphs as well as the calibration expressions themselves.

abundance ratios become more uncertain outside those intervals (see Fig. 4).

The stars' samples adopted in the calibrations are extensive enough and exhibit wide ranges of photospheric parameters, which are as extensive as those of the MILES control sample, including uncertainties. Parameter intervals covered can be seen in plots of Fig. 5 (described ahead).

We verified the atmospheric parameter sensitivity of the [Mg/Fe] differences between MR and HR results. Fig. 5 presents them as a function of T_{eff}, $\log g$ and [Fe/H] for both Mg features. There is no significant dependence on the photospheric parameters, as indicated by the linear fits (tiny linear correlation coefficients). Furthermore,

the differences are always smaller or comparable to *rms* scatter along the whole parameter scales.

Therefore, where possible, we averaged the calibrated ratios obtained from both features, in order to obtain calibrated abundance ratios as follows:

$$\overline{[Mg/Fe]^{calib}} = \left([Mg/Fe]^{calib}_{Mg5183} + [Mg/Fe]^{calib}_{Mg5528}\right)/2. \quad (6)$$

In Fig. 6, the residuals between calibrated results from the two features are plotted as a function of T_{eff}, $\log g$ and [Fe/H]. There is no systematic dependency on the stellar parameters, as it is noticed from the small linear correlation coefficients r. This supports our procedure of computing averages of $[Mg/Fe]^{calib}_{feature}$. The medium data dispersion (0.15 dex *rms*) is comparable with the typical internal error and systematic error for the calibrated ratio from Mg5528, but is slightly greater for the other feature. It is equal to the systematic error of $[Mg/Fe]^{calib}_{Mg5528}$ (±0.15 dex), but it is slightly greater than $\sigma[Mg/Fe]^{calib}_{Mg5183}$ (0.13 dex) and $\sigma\overline{[Mg/Fe]^{calib}}$ (0.10 dex).

The criterion for deciding if the calibrated [Mg/Fe] measurements of both Mg features can be averaged to obtain representative determinations is fixed by the maximum deviation acceptable between them, i.e. the condition is expressed by $|[Mg/Fe]^{calib}_{Mg5528} - [Mg/Fe]^{calib}_{Mg5183}| \leq 4\sigma\overline{[Mg/Fe]^{calib}}$ or $\Delta[Mg/Fe]_{Mg5528-Mg5183} \leq 0.40$ dex, as illustrated in Fig. 6 and adopted for calibrated HR measurements collected from duplicated sources (Section 2.2). See Section 3.5 to get details about how $\sigma[Mg/Fe]^{calib}$ was estimated. The Mg5183 determination was adopted for the stars that do not follow this condition (five dwarfs and 10 giants), because this feature provides a better precision.

After separately calibrating $[Mg/Fe]_{Mg5183}$ and $[Mg/Fe]_{Mg5528}$, using the extensive control sample, we were able to compute average or individual feature values for a great number of dwarfs and giants. In total, we measured [Mg/Fe] at MR for 437 extra MILES stars (150 dwarfs and 287 giants). This represents around 44 per cent of the whole spectral library.

3.5 Uncertainty of the mid-resolution measurements

The internal uncertainties of [Mg/Fe] are due to the MILES photospheric parameter errors and the abundance determination methods applied (EW and LPF).

We estimated the error propagation from the imprecision of T_{eff}, $\log g$ and [Fe/H] by adopting model atmospheres directly collected from the MARCS 2008 grid, whose parameters coincide with the photospheric parameters of all MILES stars possible considering the typical errors (1σ). This sample of MILES stars is composed of 135 dwarfs and 31 giants, and it has an excellent coverage in the MARCS model parameter space (distributing between 4200 and 6200 K in T_{eff}, 1.0 and 4.7 in $\log g$ and -2.10 and $+0.40$ dex in [Fe/H]). Then, we computed their abundance ratios based only on the EW method by using each Mg feature, hereafter simply $[Mg/Fe]_{atm}$. Afterwards, we compared them with those measurements obtained by adopting interpolated model atmospheres, whose parameters actually match T_{eff}, $\log g$ and [Fe/H] of the stars, naming them $[Mg/Fe]_{interpol}$. In this procedure, all [Mg/Fe] are not calibrated to the HR uniform scale, since only differences are needed for estimating errors. The deviation ($[Mg/Fe]_{atm} - [Mg/Fe]_{interpol}$) is well distributed around zero over all parameter scales, and it does not show any stellar parameter dependence. These differences at 1σ level gave us a good estimation for the global internal uncertainty due to the star's parameter errors, $\sigma[Mg/Fe]_{atm}$, which is around 0.09 dex for the Mg5183 feature and 0.10 dex for Mg5528.
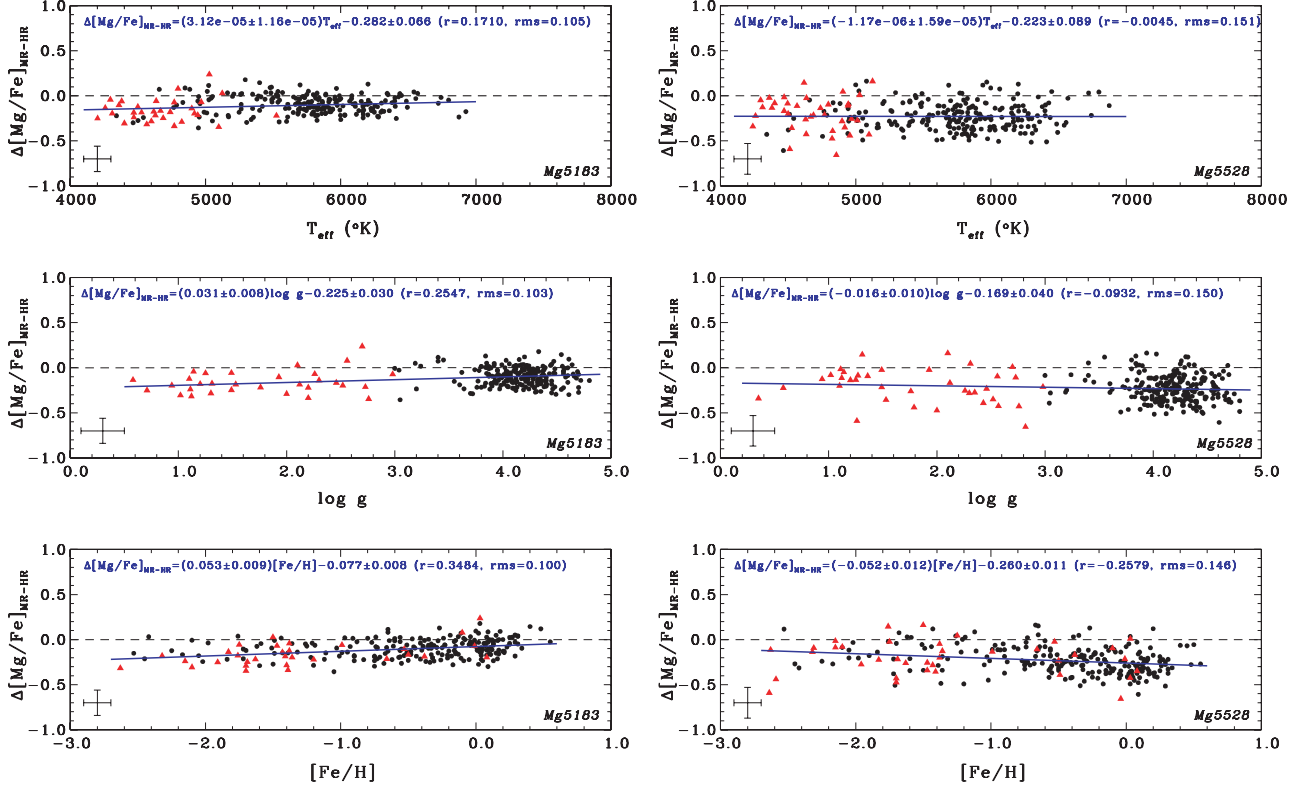
Figure 5. [Mg/Fe] differences between non-calibrated MR and calibrated HR measurements (Δ[Mg/Fe]$_{MR-HR}$ = [Mg/Fe]$_{feature}$ − [Mg/Fe]$_{HR}$) computed for the features Mg5183 (left-hand panel) and Mg5528 (right-hand panel) as a function of T_{eff}, log g and [Fe/H] distinguishing dwarfs (black filled circles) and giants (red filled triangles). Simple linear LSQ fittings between the differences and each photospheric parameter are also shown (blue solid lines). The resultant expressions, *rms* and correlation coefficient of these linear fits are displayed on the top of each graph.

The internal uncertainties in [Mg/Fe] due to the EW method itself, σ[Mg/Fe]$_{EW}$, for both Mg features were estimated by computing the propagation of the observed equivalent width errors through the relationship [Mg/Fe] versus log(EW). We noted that the EW uncertainties dominate over the propagation error from the [Mg/Fe] versus log(EW) theoretical fits. The median of the σ[Mg/Fe]$_{EW}$ asymmetric distribution for each Mg feature characterizes the typical uncertainty that it is around 0.09 dex for Mg5183 and 0.20 dex for Mg5528.

We also investigated the dependence of σ[Mg/Fe]$_{EW}$ on the atmospheric parameters. There is some correlation with [Fe/H] for Mg5183 only, where σ[Mg/Fe]$_{EW}$ is higher on average for metal-poor stars ($\sim$0.2 dex) in comparison with metal-rich stars ($\sim$0.1 dex) with a transition limit around [Fe/H] = −1.0 dex. Although a metallicity dependence is also noticed in HR measurements, as in BM05, we decided not to estimate σ[Mg/Fe]$_{EW}$ as a function of [Fe/H].

The uncertainty from the LPF method depends on how accurately the minimum of the curve is determined (see Fig. 3). Typically, this is estimated to be between 0.05 and 0.10 dex, giving a mean of σ[Mg/Fe]$_{LPF}$ around 0.075 dex. The final uncertainty due to the measurement process was computed as the mean value of the abundance uncertainties obtained with the two methods, because, although they are not completely independent, the data are treated in different ways through them. Typical value of $\sigma\overline{\text{[Mg/Fe]}}_{method}$ is 0.06 dex for Mg5183 and 0.11 dex for Mg5528. The typical final internal error for each Mg feature, 0.11 and 0.15 dex for Mg5183 and Mg5528, respectively, was obtained as the quadratic sum of σ[Mg/Fe]$_{atm}$ and $\sigma\overline{\text{[Mg/Fe]}}_{method}$.

The systematic uncertainties of calibrated MR [Mg/Fe] were estimated by comparing these values directly with HR values, such that the *rms* of deviation ([Mg/Fe]$_{feature}^{calib}$ − [Mg/Fe]$_{HR}$) represents a good estimation, i.e. for each Mg feature we have

$$\sigma[\text{Mg/Fe}]^{calib} = \left(\frac{1}{N} \sum_{i=1}^{N} ([\text{Mg/Fe}]^{calib} - [\text{Mg/Fe}]_{HR})^2 \right)^{1/2}, \quad (7)$$

where N means the number of stars in the MR versus HR comparisons for each Mg feature determination. Therefore, [Mg/Fe] recovered by Mg5183 holds an uncertainty of 0.13 or 0.15 dex when it is uniquely measured by Mg5528. When it was possible to compute [Mg/Fe] as an average from both feature determinations, its systematic error $\sigma\overline{\text{[Mg/Fe]}}^{calib}$ was estimated by quadratic mean reaching 0.10 dex. Table 3 summarizes the [Mg/Fe] uncertainties.

We also investigated the influence of the models atmosphere α-enhancement chemistry on the spectral synthesis carried out at MR by always keeping the model chemistry unchanged at each metallicity (see Section 3.1). Besides the MARCS standard models adopted in our work, there are other model classes: one named alpha-poor assuming α/Fe solar for −2.00 ≤ [Fe/H] ≤ −0.25 dex, and another denominated alpha-enhanced with [α/Fe] = +0.40 dex covering [Fe/H] from −0.75 to +0.50 dex. Thus, we performed spectral syntheses to cover four ([Fe/H], [α/Fe]) (dex, dex) combinations as following: (i) (−1.50, 0.00) and (ii) (−1.50, +0.40) with the alpha-poor ([α/Fe] = 0.00 dex) and standard ([α/Fe] = +0.40 dex) models for this metallicity, and (iii) (0.00, 0.00) and (iv) (0.00, +0.40) with the standard ([α/Fe] = 0.00 dex) and alpha-enhanced ([α/Fe] = +0.40 dex) models for this metallicity. The syntheses were applied to four stellar evolution stages: main sequence (MS) at
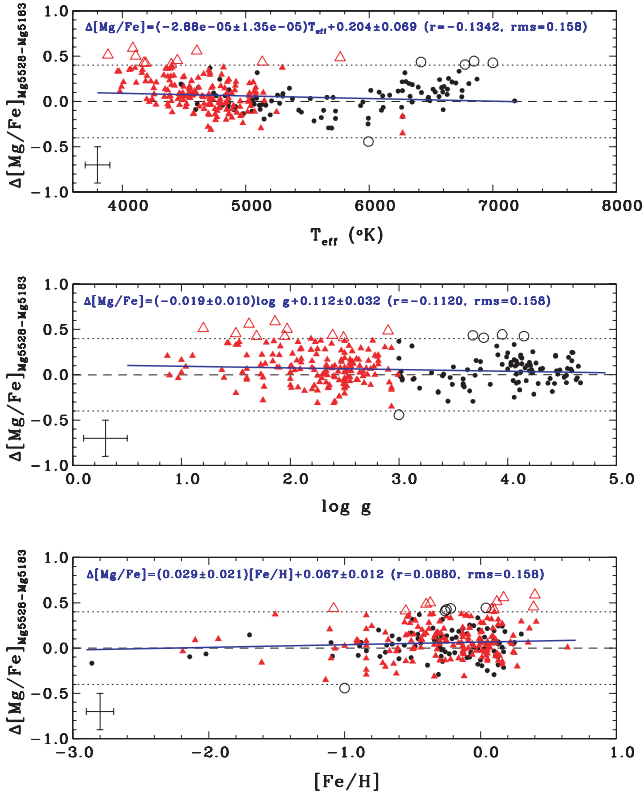
Figure 6. [Mg/Fe] differences between the calibrated measurements obtained with the two Mg features (Δ[Mg/Fe]$_{\text{Mg5528-Mg5183}}$ = [Mg/Fe]$_{\text{Mg5528}}^{\text{calib}}$ − [Mg/Fe]$_{\text{Mg5183}}^{\text{calib}}$) as a function of T_{eff}, log g and [Fe/H] for dwarfs (black filled circles) and giants (red filled triangles). LSQ linear fittings between the differences and each photospheric parameter are also shown (solid blue lines) considering the data shown as filled symbols. Two parallel dotted black lines are drawn to representing the 4σ $\overline{\text{[Mg/Fe]}^{\text{calib}}}$ as a maximum acceptable deviation for Δ[Mg/Fe]$_{\text{Mg5528-Mg5183}}$ (details in the end of Section 3.5). The black open circles represent the dwarfs and red open triangles the giants for which average abundance ratios were not computed based on the 4σ criterion. These stars are not considered in the LSQ fittings.

$T_{\text{eff}} = 5000$ K and log $g = 4.5$, turn-off MS at $T_{\text{eff}} = 6000$ K and log $g = 4.0$, sub-giant at $T_{\text{eff}} = 5000$ K and log $g = 3.5$, red giant branch at $T_{\text{eff}} = 4500$ K and log $g = 1.0$. However, just the red giant stage could be adopted for the solar metallicity due to a limitation of the MARCS alpha-enhanced class coverage. Afterwards, we directly compared the equivalent widths of each Mg feature measured on theoretical spectra that have been computed for each

metallicity–α-enhancement combination but assuming two different model classes.

At [Fe/H] $= -1.50$ dex, it is noticed that the EW variations of both Mg features are very acceptable within typical uncertainties, i.e. <8 per cent for the MS and sub-giant stages and <3 per cent for the turn-off and red giant stages that are translated into [Mg/Fe] abundance ratio changes smaller than around 0.10 and 0.05 dex, respectively. At solar metallicity, the EW variations of red giant stage (the only one analysed) are smaller than 7 per cent for Mg5183 (or about 0.09 dex in [Mg/Fe]) and 20 per cent for the Mg5528 feature (or ∼0.2 dex in [Mg/Fe]). Therefore, it is viable to perform spectral synthesis at MR by fixing the model atmosphere chemistry and changing the α-element abundances to cover a large range of [α/Fe] values as it was done in the current work.

However, a conservative variation of $\pm$0.2 dex for [α/Fe] in the spectral syntheses done under fixed model atmosphere chemistries could be assumed in order to figure out which abundance ratio determinations would be considered as extrapolations based on the α-enhancement compatibility. Concerning the MARCS standard models adopted and taking into account the uncertainties of [Mg/Fe]$^{\text{calib}}$, we have found 33 stars, which represent just 7.5 per cent of all MR determinations and are identified in the catalogue (Section 4). Consequently, the [Mg/Fe] of each case might have a less accuracy in the sense it was based on a model atmosphere whose chemistry does not exactly follow the abundances of α-elements adopted in the spectral synthesis. These cases include those extrapolations over the Mg feature calibrations themselves (Section 3.4).

3.6 Coverage of the MR measurements

There are 843 MILES stars with catalogued atmospheric parameters within the MARCS 2008 grid. From those, 308 already had [Mg/Fe] measurements from HR studies (Section 2). The 535 residual stars were spectroscopically analysed by us at MR. The MR determinations cover wide ranges in atmospheric parameters (see Figs 8 to 11 described in Section 4), reaching 81.7 per cent efficiency or completeness level inside the MARCS parameter space when the stars with HR data are not considered. Rather than be uniform over all scales, our measurements actually complement the HR data. However, depending on the region, one Mg feature works better than the other. Section 4 presents a more extensive discussion about the parametric coverage of all MR and HR determinations.

In general, the Mg5183 feature does not work well on the coldest stars ($T_{\text{eff}} < 4000$ K) due to the presence of strong molecular absorptions of TiO and MgH as well. Mg5528 is not satisfactorily applied for the hottest giants ($T_{\text{eff}} > 5500$ K), since this feature becomes too weak and it is practically insensitive to abundance variation in

Table 3. Typical uncertainties of [Mg/Fe] (dex unity) from our MR measurements, showing the internal errors for the Mg5183 and Mg5528 features due to the photospheric methods adopted (pseudo-equivalent widths, EW and LPF) and stellar atmospheric parameter errors. The total uncertainty of non-calibrated [Mg/Fe]$_{\text{feature}}$ and the systematic error of calibrated [Mg/Fe]$^{\text{calib}}$ for each Mg feature is presented, respectively, in the last and penultimate rows.

No.		Mg5183 (dex)	Mg5528 (dex)	Both (dex)	Notes
1	σ[Mg/Fe]$_{\text{EW}}$	0.09	0.20	–	From the EW method
2	σ[Mg/Fe]$_{\text{LPF}}$	0.075	0.075	–	From the LPF method
3	σ[Mg/Fe]$_{\text{method}}$	0.06	0.11	–	From rows one and two variance averaged
4	σ[Mg/Fe]$_{\text{atm}}$	0.09	0.10	–	Due to the photospheric parameter errors
5	σ[Mg/Fe]$_{\text{feature}}$	0.11	0.15	–	Internal errors from rows three and four combined in quadrature
6	σ[Mg/Fe]$_{\text{feature}}^{\text{calib}}$	0.13	0.15	0.10	Systematic errors (from HR comparisons), variance averaged in the last column

Table 4. The MILES [Mg/Fe] catalogue for field stars. First column presents the star identification in the MILES data base. The identification in the CaT library (Cenarro et al. 2002) is in the second column. The stars' names in other catalogues are shown in the third column. The stellar photospheric parameters in MILES are listed from the fourth to sixth columns. [Mg/Fe] is shown in the seventh column together with its error in the eighth column. Notes about the source of each [Mg/Fe] measurement are written in the last column identifying its origin, i.e. from the HR compilation (HR) or our MR measurements (mr), as well as the HR work, BM05 or other(s) listed in Table 1, the Mg feature(s) adopted in each stellar MR measurement, and if the MR measurement represents an α-enhancement model atmosphere extrapolation as described in Section 3.5 (designated by *). This is a sample of the full table, which is available with the online version of the article (see Supporting Information).

No. MILES	No. CaT	Star name	$T_{\rm eff}$ (K)	$\log g$	[Fe/H] (dex)	[Mg/Fe] (dex)	σ[Mg/Fe] (dex)	Notes
0081F		BD−010306	5650	4.40	−0.90	+0.40	0.05	HR BM05
0266F		BD−011792	4948	3.05	−1.05	+0.71	0.20	HR T98
0505F	677	BD+012916	4238	+0.35	−1.47	+0.37	0.20	HR T98
0329F		BD−032525	5750	3.60	−1.90	+0.41	0.07	HR BM05
0777F		BD+044551	5770	3.87	−1.62	+0.42	0.07	HR BM05
0327F		BD−052678	5429	4.43	−2.14	+0.41	0.10	mr BothMg
0569F		BD+053080	4832	4.00	−0.88	+0.55	0.10	mr BothMg
0142F		BD+060648	4400	1.02	−2.10	+0.52	0.20	HR T98
0144F		BD−060855	5283	4.50	−0.70	−0.01	0.05	HR BM05
0537F		BD+062986	4450	4.80	−0.30	+0.06	0.13	mr Mg5183

these cases. In particular, Mg5183 gives reliable abundance measurements for dwarfs and giants with temperatures between 4000 and 8000 K, while Mg5528 basically works on dwarfs with 3500 up to 8000 K. However, for giants, Mg5528 can only be applied with great confidence for $3600 \leq T_{\rm eff} \leq 5500$ K. Both Mg features can be used in the whole metallicity range.

In specified cases, the spectral synthesis does not work on a single or both features, due to line saturation, non-reproduction of spectrum continuum, extrapolation on the [Mg/Fe] versus log (EW) and/or $rms_{\rm LPF}$ versus [Mg/Fe] relationship, incompleteness of line lists (mainly TiO bands) and low-quality spectra in some cases. The continuum and EW/LPF extrapolation cases do not exhibit any stellar parametric dependence for Mg5183. On the other hand, we noted the cases of line saturation and incomplete line list occur in metal-rich cold stars ([Fe/H] > −1.0 dex with $T_{\rm eff}$ < 4000 K) for both features. A few of those non-reproduced spectral cases (that sum in total 79 dwarfs and 115 giants for Mg5183 plus 60 dwarfs and 97 giants for Mg5528) could be fixed, excepting those due to the incompleteness of line lists: eight cases for Mg5183 (five dwarfs and three giants), and 15 cases for Mg5528 (five dwarfs and 10 giants). The line saturation effect was solved by adopting a spline fit on the EW method and sometimes a smaller number of models (nine cases in total).

4 THE MILES MAGNESIUM ABUNDANCE CATALOGUE

We have obtained [Mg/Fe] covering a bit more than 3/4 (more precisely 752 stars or 76.3 per cent) of the MILES stellar spectrum library (411 dwarfs and 341 giants, respectively, around 76 per cent and 77 per cent of their totals) that are suitable for SSP modelling, i.e. the typical systematic uncertainty of [Mg/Fe] is 0.105 dex on average over our whole catalogue. The stars' coverage in the four-dimensional parameter space of MILES $T_{\rm eff}$, $\log g$, [Fe/H] and [Mg/Fe] is extensive, as discussed in this section. If we only consider the MILES stars with complete sets of photospheric parameters that sum 946 objects (Cenarro et al. 2007), the coverage reaches 79.5 per cent.

The compiled [Mg/Fe] catalogue of MILES is presented in Tables 4 and 5 for field and cluster stars, respectively. These are samples of the full tables; the whole catalogue is available with the online version of the article (see Supporting Information). Basically, the catalogue tables provide the [Mg/Fe] values with their individual errors together with the sources from where they have been obtained [i.e. the reference in case it has been compiled from HR works or the Mg feature(s) when it is an MR measurement].

Fig. 7(a) shows the stars' coverage over the modified H-R diagram $\log g$ versus $T_{\rm eff}$, Fig. 7(b) explores the coverage around the

Table 5. The MILES [Mg/Fe] catalogue for star cluster stars (as in Table 4). The cluster names and types are in third and fourth columns. This is a sample of the full table, which is available with the online version of the article (see Supporting Information).

No. MILES	No. CaT	Cluster name	Type	Star name	$T_{\rm eff}$ (K)	$\log g$	[Fe/H] (dex)	[Mg/Fe] (dex)	σ[Mg/Fe] (dex)	Notes
0920C	006	Coma Ber	Open	HD 107276	7972	4.21	−0.05	+0.29	0.15	mr Mg5528
0921C	007	Coma Ber	Open	HD 107513	7409	4.25	−0.05	+0.32	0.15	mr Mg5528
0901C	016	Hyades	Open	HD 025825	5992	4.41	+0.13	−0.09	0.10	mr BothMg
0902C	017	Hyades	Open	HD 026736	5657	4.45	+0.13	−0.24	0.10	mr BothMg*
0904C		Hyades	Open	HD 027383	6098	4.28	+0.13	+0.03	0.10	mr BothMg
0905C	023	Hyades	Open	HD 027524	6622	4.28	+0.13	−0.16	0.15	mr Mg5528*
0906C	025	Hyades	Open	HD 027561	6742	4.24	+0.13	+0.03	0.20	HR T98
0907C		Hyades	Open	HD 027962	8850	3.80	+0.13	−0.09	0.20	HR T98
0908C	029	Hyades	Open	HD 028483	6486	4.30	+0.13	+0.01	0.20	HR T98
0909C		Hyades	Open	HD 028546	7626	4.11	+0.13	−0.23	0.15	mr Mg5528*
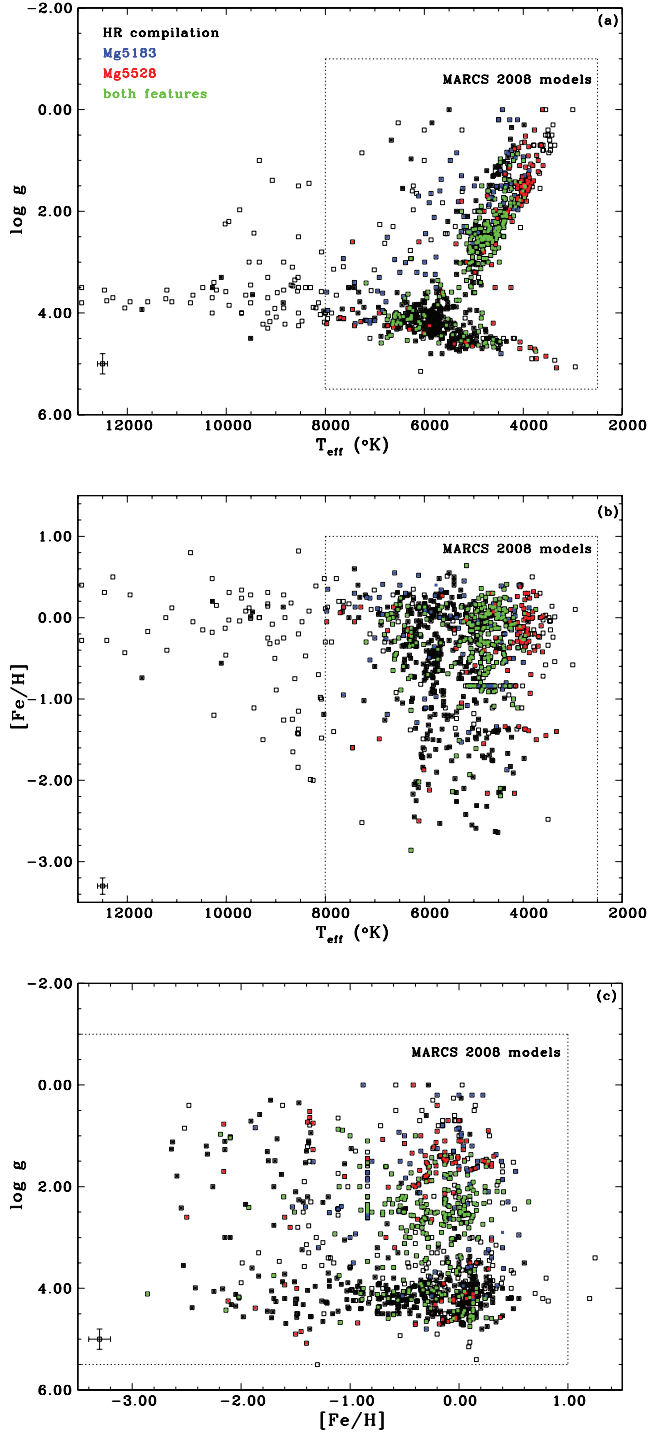
Figure 7. Coverage of the MILES stars with [Mg/Fe] in the photospheric parameter space: (a) modified H-R diagram log g versus $T_{\rm eff}$ (top panel), (b) [Fe/H] versus $T_{\rm eff}$ plane (middle panel) and (c) log g versus [Fe/H] projection (bottom panel). The MILES stars with abundance ratios from HR studies are shown as black filled symbols, and the stars with MR measurements from this work as colour filled symbols (blue designating determinations based on the Mg5183 feature only, red on Mg5528 only and green on both Mg features combined). The library stars without [Mg/Fe] are drawn as open symbols. The MARCS 2008 grid extension is also represented in each panel.
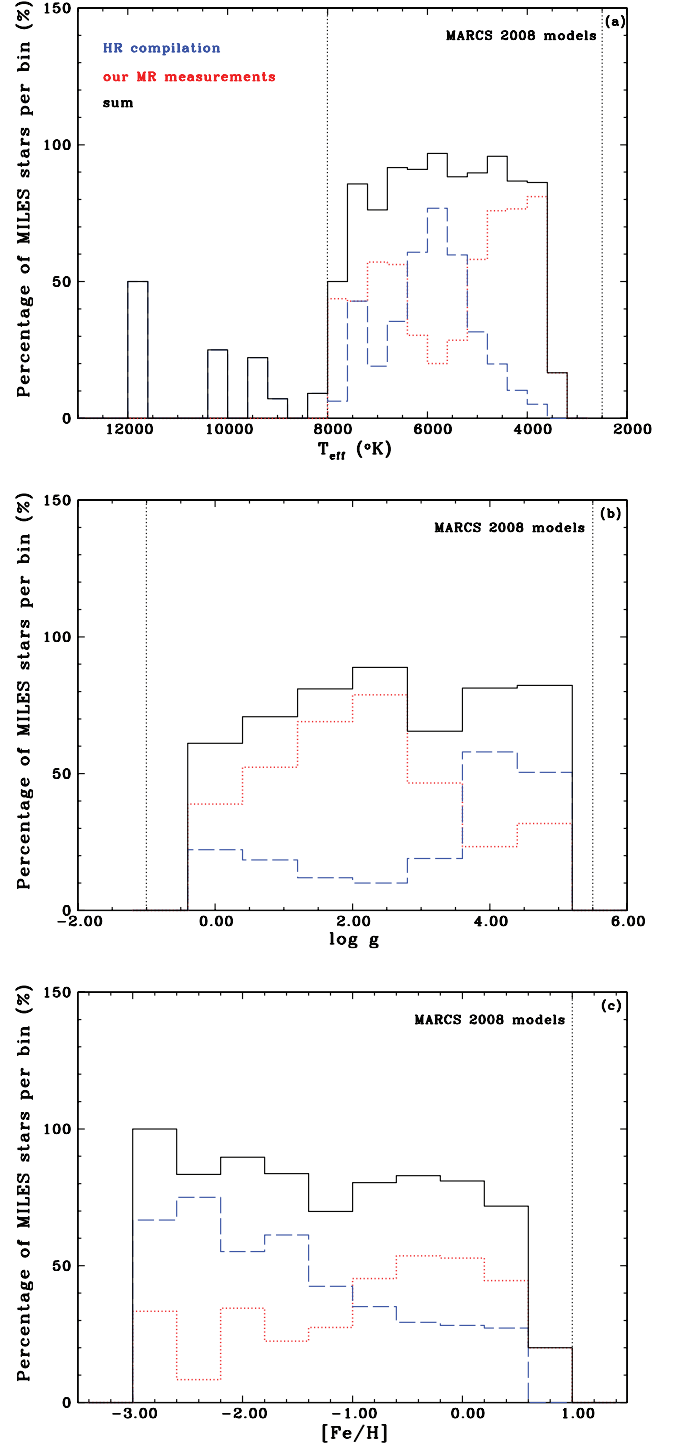
Figure 8. Distribution of the MILES stars with [Mg/Fe] over the photospheric parameter space: (a) effective temperature scale (top panel), (b) surface gravity scale (middle panel) and (c) metallicity scale (bottom panel). The percentage number per bin of the MILES stars with abundance ratios from HR studies is shown by blue dashed line, and the percentage number of stars with our MR measurements by the red dotted line. The sum of both is represented by the black solid line. The adopted bins are equal to four times the parameter uncertainties. The coverage of the MARCS 2008 grid of model atmospheres is also drawn in each panel.
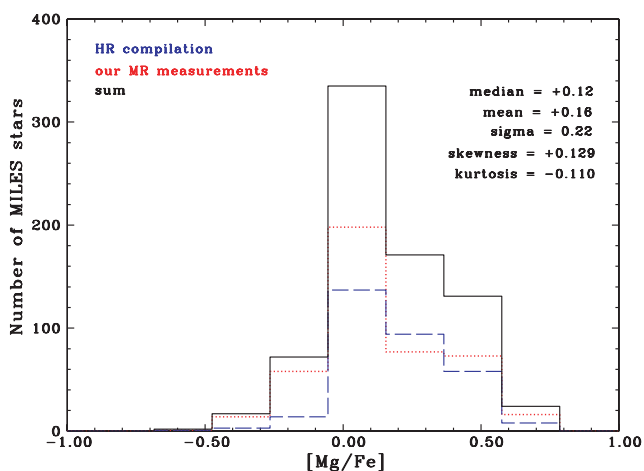
Figure 9. Distribution of abundance ratios over the MILES [Mg/Fe] catalogue built up in this work. The histogram of stars with data from the HR compilation is shown by blue dashed line, and the distribution of our MR measurements by the red dotted line. The sum of both data sets is plotted by the black solid line. The adopted bin is two times the average uncertainty of [Mg/Fe] over the whole catalogue (2σ[Mg/Fe] = 0.21 dex). The median, mean, sigma, skewness and kurtosis of the accumulated distribution are also informed.

projection [Fe/H] versus $T_{\rm eff}$ and Fig. 7(c) presents it on the plane $\log g$ versus [Fe/H]. The MILES stars with and without [Mg/Fe] are represented in all these plots, in which the parametric extension of MARCS 2008 grid is also drawn. The stars with [Mg/Fe] are distinguished according to the origin of their measurements. Fig. 8 exhibits the distribution of MILES [Mg/Fe] catalogue over the $T_{\rm eff}$, $\log g$ and [Fe/H] scales.

The sum of all measurements (HR plus MR) shows fairly flat distributions across the photospheric parameter space covered by the MARCS models (histograms of Fig. 8). The [Mg/Fe] HR data are distributed along the MS basically from $T_{\rm eff}$ about 4500 up to around 10000 K and on the giant branch mainly from 4000 up to 5500 K, as seen in Fig. 7(a). Our MR measurements have a wide distribution over the plane $\log g$ versus $T_{\rm eff}$; however there are some deficiencies such as in the low MS, the red giant branch tip and the hottest giants. The histogram of $T_{\rm eff}$ (Fig. 8a) shows a peak at 6200 K for the HR compilation data while the MR measurements have a gradual increasing from 8000 to 4200 K. There is a wide coverage over the whole MILES metallicity scale for both HR and MR data sets. In the projection [Fe/H] versus $T_{\rm eff}$ (Fig. 7b), we notice a predomination of the HR data between 5000 and 6000 K. In the plane $\log g$ versus [Fe/H] (Fig. 7c), the dwarfs are well covered by the HR data. The MR distribution dominates in the metal-rich regime and the HR data compilation dominates in the metal-poor regime, complementing each other well (see also Figs 9c and 11). Whilst the HR measurements provide mostly data for MILES dwarfs, reaching the completeness maximum around $\log g = 4.0$ (Fig. 8b), our MR measurements contribute significantly to giants, with a gradual decrease from $\log g = 2.5$ to 0.0.

Specifically for the MR measurements that were done within the limits of MARCS 2008 grid as shown in Figs 8 and 9, the highest completeness over the $T_{\rm eff}$ scale occurs around 4000 K whilst the smallest is at 6000 K. The maximum coverage in the gravity scale occurs at $\log g = 2.5$ and the minimum is around $\log g = 4.0$. The maximum of completeness over the metallicity scale is at -0.40 dex and the minimum occurs at [Fe/H] $= -2.4$ dex.

Fig. 9 presents the MILES catalogue's [Mg/Fe] distribution itself, which is highly asymmetric around the solar ratio showing a sharp decline towards negative values and a shallow decreasing towards overenhanced ratios (skewness $= +0.129$). The average of [Mg/Fe] is $+0.16$ dex having a standard deviation of 0.22 dex. The median of distribution is $+0.12$ dex. The distribution of our MR measurements matches well the HR data distribution (both sets on a same homogeneous scale). The median and average of HR data are $+0.16$ dex and $+0.19$ dex ($1\sigma = 0.19$ dex), respectively, whilst they are $+0.09$ dex and $+0.14$ dex ($1\sigma = 0.24$ dex) for the MR measurements. The positive asymmetry also exists in both distributions: the HR data have skewness equal to $+0.081$ and for the MR measurements it is $+0.220$. The difference between them is that the HR data present a peaked distribution (kurtosis $= +0.178$) whilst the MR values show a less peaked distribution (kurtosis $= -0.279$). The MILES stars, therefore, now have [Mg/Fe] measurements covering a range that is not restricted to the solar abundance ratio.

Fig. 10 plots [Mg/Fe] as a function of [Fe/H]. We can affirm that the MR measurements follow very well the solar neighbourhood global pattern of the HR data, i.e. our determinations at medium spectral resolution statistically recover with acceptable accuracy this abundance ratio along the whole metallicity scale. At a given [Fe/H], the scatter of [Mg/Fe] is slightly larger when it is measured by using Mg5183 than when Mg5528 or both features combined are adopted. However, the systematic error on the [Mg/Fe] value is smaller when the Mg5183 feature is used (see also Section 3.5). In the MILES data set, there is a mix of stars from different kinematic populations of our Galaxy distributed over the thin and thick discs as well as the halo. Several recent studies based on homogeneous HR spectroscopic analyses have shown the intrinsic dispersion of [Mg/Fe] or [α/Fe] at a fixed [Fe/H] inside a particular disc population seems to be really small indeed (e.g. Chen et al. 2000; Mishenina et al. 2004; Bensby et al. 2005; Reddy et al. 2006; Bensby et al. 2010; Nissen & Schuster 2010) but Neves et al. (2009) have found the opposite result. On the other hand, halo stars ([Fe/H] ≤ -1.0 dex) exhibit great spread in the plane [Mg/Fe] versus [Fe/H] (e.g. Stephens & Ann Merchant 2002; BM05). It is not the scope of the current work to explore the details about the elemental abundances over the Galaxy's kinematic components. These issues may be the central subject of a future work.

Fig. 11 shows that there is good coverage of [Mg/Fe] over the $T_{\rm eff}$ and $\log g$ scales (uniformly from 4000 to 5500 K and nearly uniform along whole gravity scale), with poorest completeness at the lowest and highest temperature ranges. In addition, there is a dearth of stars with sub-solar [Mg/Fe] around $T_{\rm eff} = 6000$ K, and for giant stars with low $\log g$ values.

Table 6 shows the stellar parameter coverage of the MILES [Mg/Fe] catalogue over the HR and MR data, and dwarfs and giants as well. Table 7 summarizes the catalogued data presenting the number of HR and MR measurements around dwarfs and giants together with their uncertainties.

5 COMPARISON WITH THEORETICAL MODEL PREDICTIONS

In previous stellar population studies, there have been attempts to account for variations in element abundance ratios by the use of response functions that give the dependence of line-strength indices on just a single chemical element. These response functions are calculated by adopting model atmospheres of, usually, just three or four different stars. Examples include the models of Weiss, Peletier & Matteucci (1995), Tripicco & Bell (1995), K05, Coelho et al.
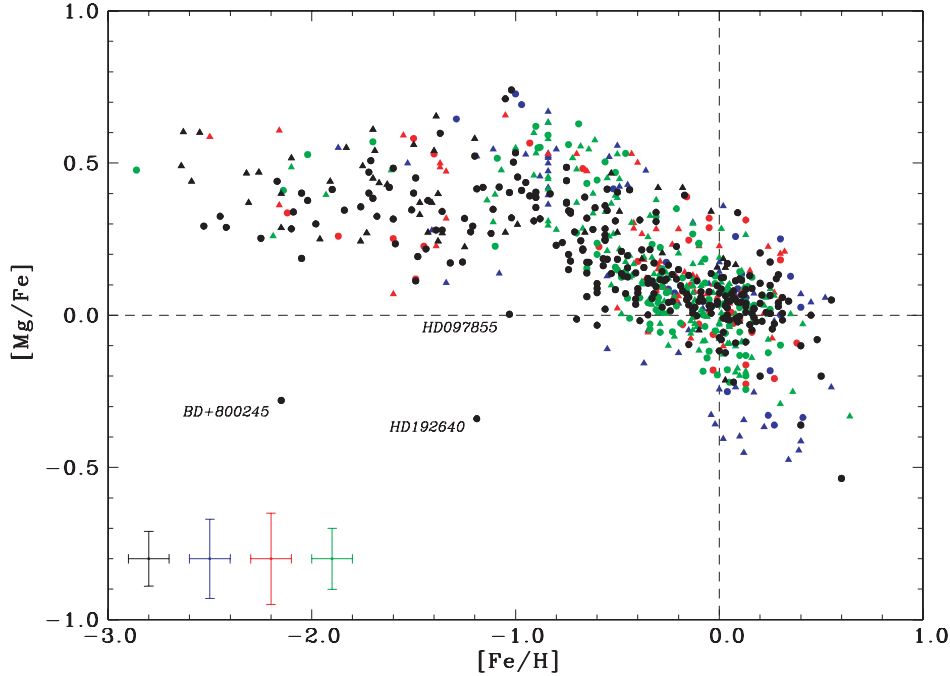
Figure 10. [Mg/Fe] as a function of [Fe/H] showing all MILES stars with [Mg/Fe] from the HR compilation as black symbols and MR measurements as colour symbols (blue designating determinations based on the Mg5183 feature only, red on Mg5528 only and green on both Mg features combined). Dwarfs (log $g \leq 3.0$) are shown as circles and giants as triangles. The weighted average uncertainties for each data group (HR, Mg5183, Mg5528 and both features combined) are illustrated on the bottom left corner. Three chemically peculiar stars are also identified.

(2005) and Serven, Worthey & Briley (2005) ([α/Fe] = 0.0 and +0.3 dex models, effects on many spectral lines of many elements tested individually). Such models have been used in various studies to interpret the spectra of galaxies and globular clusters (e.g.

Table 6. Stellar parameter coverage of the MILES [Mg/Fe] catalogue for the HR and MR data distinguishing dwarfs (log $g \geq 3.0$) and giants (log $g < 3.0$).

Class	$T_{\rm eff}$ (K)	log g	[Fe/H] (dex)	[Mg/Fe] (dex)
HR				
Dwarfs	4342, 11704	3.0, 4.80	−2.53, +0.60	−0.54, +0.74
Giants	3902, 6666	0.0, 2.98	−2.64, +0.10	−0.21, +0.65
MR				
Dwarfs	3330, 7972	3.0, 5.08	−2.86, +0.41	−0.36, +0.73
Giants	3600, 7636	0.0, 2.99	−2.50, +0.64	−0.47, +0.67

Table 7. The distribution of HR and MR measurements around dwarfs (log $g \geq 3.0$) and giants (log $g < 3.0$) in the MILES [Mg/Fe] catalogue. The weighted average uncertainty σ[Mg/Fe] is also presented for each group of measurements.
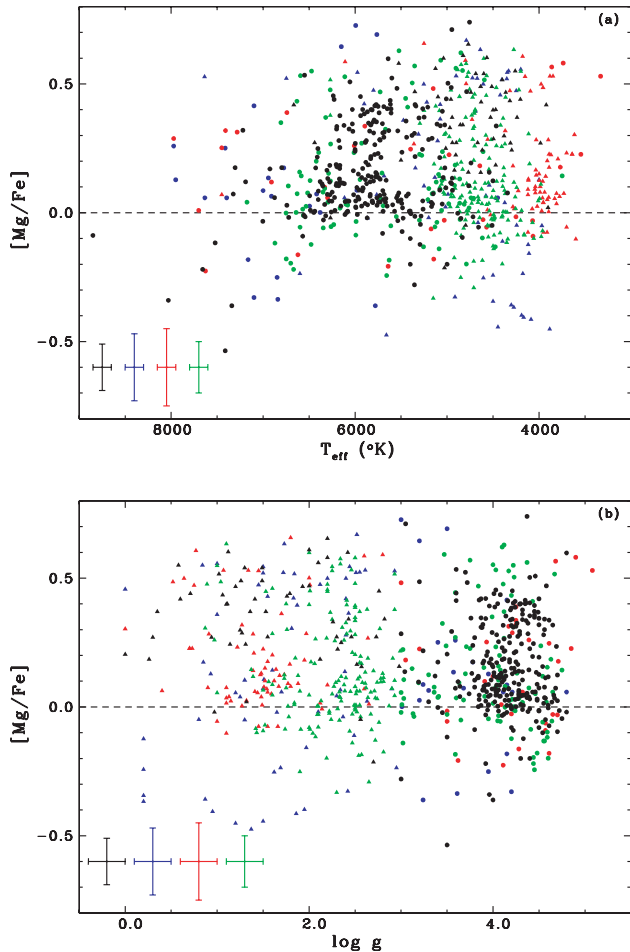
Data source	Dwarfs	Giants	Total	σ[Mg/Fe] dex
HR	263	52	315	0.09
Mg5183	23	62	85	0.13
Mg5528	31	69	100	0.15
Both features	96	156	252	0.10
MR sum	150	287	437	0.12
Total sum	411	341	752	0.105

Vazdekis, Peletier & Beckman 1997; Trager et al. 2000b; Proctor & Sansom 2002; Denicoló et al. 2005; Lee & Worthey 2005, Schiavon 2007, Coelho et al. 2007; Pipino et al. 2009b; Smith, Lucey & Hudson 2009a). The accuracy of those response functions, however, has not been calibrated or tested empirically.

In the present paper, variations in [α/Fe] are characterized by measuring Mg abundances in *real stars* and using this to represent α-elements in general. In this section, we compare the effects on Lick indices of these [α/Fe] ratios derived from observations with theoretical predictions for how Lick indices are expected to change with variations in [α/Fe]. The models of K05 are used for this comparison, since they were used in many of the above referenced studies of galaxies. Equation (7) from Thomas et al. (2003) shows how we can predict changes in spectral line indices with changing composition for lines that tend to zero strength as the element abundance dominating that line tends to zero. Other line indices (e.g. Hγ, Hδ, G4300, Fe4383) take both negative and positive values, due to lack of a real continuum definition in complex star spectra. This particularly affects indices in the blue part of the spectrum where the continuum level changes rapidly with wavelength in long-lived, late-type stars. For these indices we adopt the formalism given in equation (3) of K05, which modifies fluxes rather than line strengths. For molecular bands and negative going lines differences in indices are compared, whereas for positive absorption lines ratios are used for comparisons.

The catalogue of MILES atmospheric parameters (Cenarro et al. 2007) was cross-correlated with the measured [Mg/Fe] cases and with the models of K05 to find samples of stars useful for comparing observations with models, in order to test their agreement. There are then 31 stars in the MILES library whose surface temperature and gravity are the same as that of the turn-off star model ($T_{\rm eff}$ = 6200 K, log g = 4.1) given in table 13 of K05, within observational errors ($\Delta T_{\rm eff}$ = ±100 K, Δlog g = ±0.2). Amongst these 31 stars

Figure 11. Distribution of [Mg/Fe] in our catalogue over the scales of effective temperature (truncated at 9000 K) in the top panel (a), and surface gravity in the bottom panel (b). The notations are those adopted in Fig. 10.

and cool-dwarf stars. These deviations will be explored in future work. In general, we see from Fig. 12 that the observed [Mg/Fe] abundances reported in this paper show the trends expected for Mg- and Fe-sensitive features, when compared to models from K05. Other indices and comparisons with models will be discussed more extensively in a future paper.

6 FURTHER APPLICATIONS TO THE ANALYSIS OF STELLAR POPULATIONS

From now on, it will be possible to build up new semi-empirical SSP models by adopting the MILES star spectrum library in order to more confidentially cover a range of values of metallicity and magnesium-to-iron abundance ratio for some ages greater than 1 up to 14 Gyr. This is one of the important further applications based on the results of this work that is scheduled by our group which has experience in studying stellar populations. The MILES stars can be now selectively collected from the library taking into account their characteristics in a more extensive parameter space, i.e. [Fe/H], [Mg/Fe], log g and $T_{\rm eff}$, to represent different SSPs for given sets of age, [Fe/H] and [α/Fe]. Magnesium may be considered a proxy of the α-elements and consequently [α/Fe] might be represented by [Mg/Fe].

There are some caveats to be aware of for using the present catalogue results. The measurements made and compiled in the present catalogue represent [Mg/Fe] well, as our tests of the spectral measurements show, considering all α-element or only Mg variations. However, it is important to be aware that not all α-elements may behave in exactly the same way in different populations. This needs to be considered when applying the present catalogue to stellar population studies. Other caveats are that [Mg/Fe] obtained through the MR calibrations applied for stars whose parameters lay outside the control sample coverage might be more uncertain than the other determinations, and that we warn the abundance ratios derived from the α-enhancement model atmosphere extrapolations should be used with certain precaution too. Caveats aside, making the approximation that [Mg/Fe] can be used to represent [α/Fe] is a significant improvement over the scaled solar assumption only. There is a great deal of interest in uncovering the information contained in non-solar abundance ratios. Therefore, we next illustrate how the catalogue may be used to generate SSPs with empirically determined non-solar [α/Fe] abundance ratios.

In this further step of our work, it will be necessary to take into account reliable cross-matching between theoretical isochrones for non-solar ratios and real stars. Basically, the dwarf and giant stars with known Mg/Fe ratio that are collected from MILES in order to represent a given SSP must be selected to precisely have on average the SSP's [Fe/H] and [Mg/Fe]. Moreover, the selected stars must be well sampled along the main evolutionary stages of an isochrone. The stars must be sufficiently close to the isochrones taking into account the errors in log g and $T_{\rm eff}$ in order to be included and weighted in the computation of SSP-integrated colours and spectra. It will be also necessary to generate additional stellar spectra for some non-completely represented stages by interpolating the MILES spectra in its four-dimensional parameter space. Other approaches can be employed to extend the coverage of the SSP sets (age, [Fe/H], [α/Fe]) such as evaluating the behaviour of integrated observational properties of the SSPs at specified metallicities as a function of [α/Fe] to computing and applying corrections to the SSP observables for a larger range of parameters. Therefore, we will be able to construct a large set of single-age single-metallicity

are two that also have the same chemical composition as the model star ([Fe/H] = 0 dex, [α/Fe] = 0 dex), within observational errors (Δ[Fe/H] = $\pm$0.1 dex, Δ[α/Fe] = $\pm$0.06 dex). This allows us to use one of these two stars as a base with which to normalize the other stars in order to show how changes in chemistry affect changes in indices, in a relative way. Model stars can then be generated to match the 31 MILES stars and normalized by the model given in table 13 of K05. To generate the model star indices the equations were first applied to correct to a specific overall metallicity (using column 14 of K05), then the equations were applied again to correct to a specific [α/Fe] ratio, modifying for all the α-elements modelled by K05. Similarly, 13 cool giant stars and seven cool dwarfs can be compared using tables 14 and 12 from K05, respectively, for solar composition models. In this way, we can compare normalized observations with normalized model predictions to see if the observations agree with previously used methods of varying [α/Fe] ratios in stellar population studies.

Examples of these comparisons are shown in Fig. 12 for Fe- and Mg-sensitive indices. Fe-sensitive features in general behave as expected in that the observed changes agree well with the predicted ones. Mg-sensitive features also show quite a good one-to-one agreement, but with scatter in excess of that expected from the observational errors. There is some suggestion of a slight systematic deviation below the one-to-one line in the case if Mgb in turn-off

single-α-enhanced stellar population models. This will open new prospects for SSP modelling and evolutionary population synthesis.

Table 8 presents a set of age, [Fe/H] and [α/Fe] combinations (36 in number) for which there are sufficient number of dwarfs and giants in our MILES [Mg/Fe] catalogue to be more consistently selected to construct SSPs by adopting scaled solar and α-enhanced isochrones with those properties. Basically, in this approach, the selection of MILES stars for each metallicity value is done taking into account 1σ or 2σ variation depending on the star's position in the H-R diagram. The stars are also collected having [Mg/Fe] values around 1σ[Mg/Fe] and 2σ[Mg/Fe] of each isochrone's α-enhancement. The weighted uncertainty of the abundance ratio in the whole MILES [Mg/Fe] catalogue is 0.105 dex (1σ) and σ[Fe/H] = 0.10 dex in MILES. We also consider variations in the isochrones' ages, which were estimated basically through plots of isochrones with distinct ages that are not shown in this section.

The Dartmouth isochrone models (Dotter et al. 2008) have been adopted as reference to match the stars' positions with isochrones in the HR diagram log g versus $T_{\rm eff}$. The Dartmouth models are a collection of scaled solar and α-enhanced isochrones that spans a range of [Fe/H] from -2.5 to $+0.5$ dex, [α/Fe] from -0.2 to $+0.8$ dex (for [Fe/H] ≤ 0.0 dex) or -0.2 to $+0.2$ dex (for [Fe/H] > 0.0 dex), with 0.2 dex steps, and initial helium mass fractions from

$Y = 0.245$ to 0.40. Their stellar evolution tracks were computed for masses from 0.1 to 4 M$_{\odot}$, allowing isochrones to be generated for ages as young as 250 Myr up to as old as 15 Gyr.

Fig. 13 shows examples of isochrone-based plots by using Dartmouth (Dotter et al. 2008) and BaSTI (Pietrinferni et al. 2004) models for 4 Gyr, [Fe/H] around zero and three distinct α-enhancements.

The BaSTI scaled solar data base (Pietrinferni et al. 2004) covers stellar evolution models for masses between 0.5 and 10 M$_{\odot}$ in a wide metallicity range (10 values of [Fe/H] from -2.27 to $+0.40$ dex). The initial He mass fraction ranges from $Y = 0.245$, for the more metal-poor composition, up to 0.303 for the more metal-rich one. For each adopted chemical composition, the evolutionary models were computed without (called canonical models) and with overshooting from the Schwarzschild boundary of the convective cores during the central H-burning phase. The stellar models are used to compute isochrones in a wide age range, from 30 Myr up to 15 Gyr. The overshooting models provide a better match to the observations at [Fe/H] around solar, and for ages equal and higher than 4 Gyr. Besides these models, BaSTI α-enhanced models were computed for [α/Fe] fixed at $+0.4$ dex and 11 values of iron metallicity between -2.62 and $+0.05$ dex (Pietrinferni et al. 2006).

Fig. 14 presents a good example of cross-matching between a group of MILES stars and an isochrone to proceed to a reliable
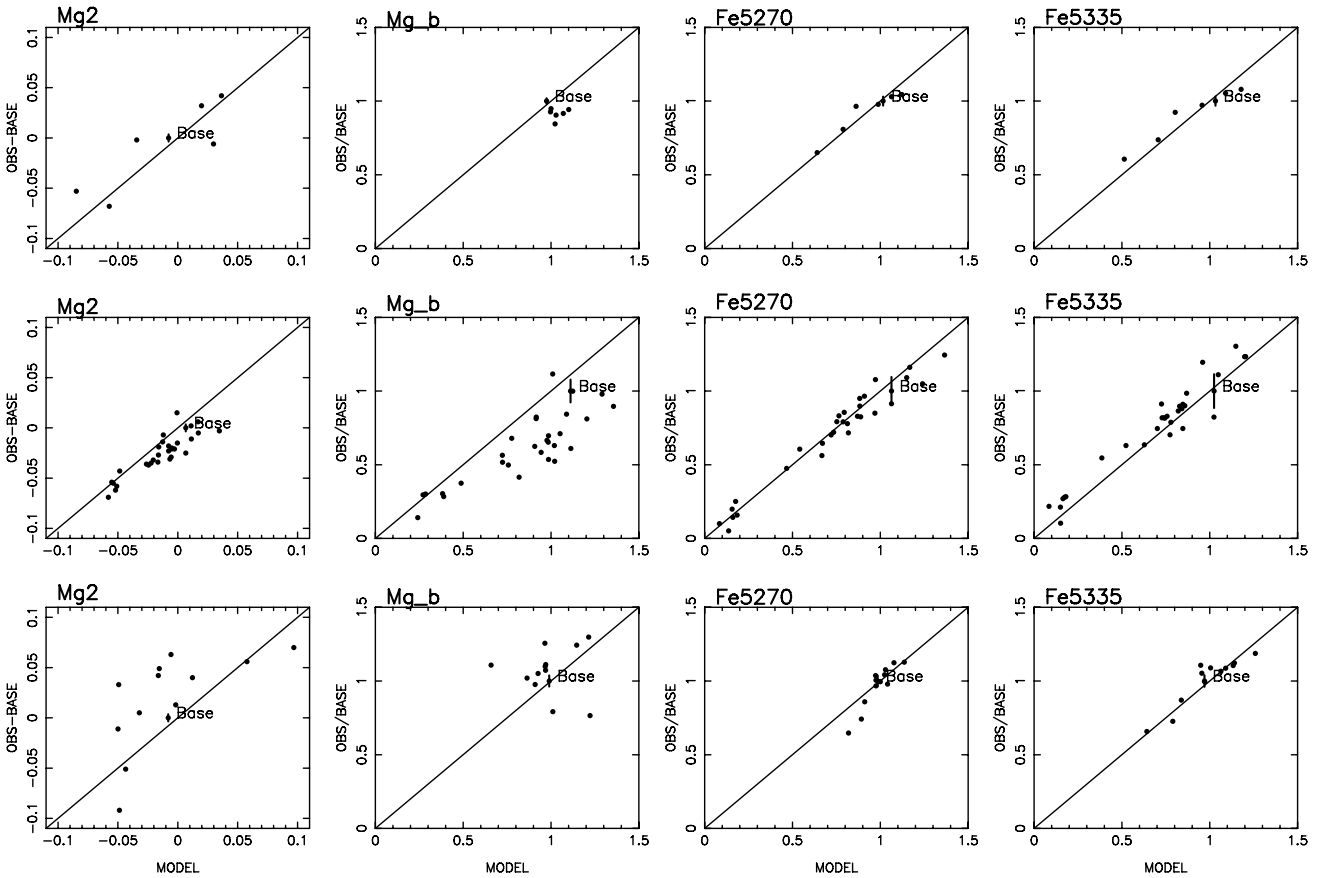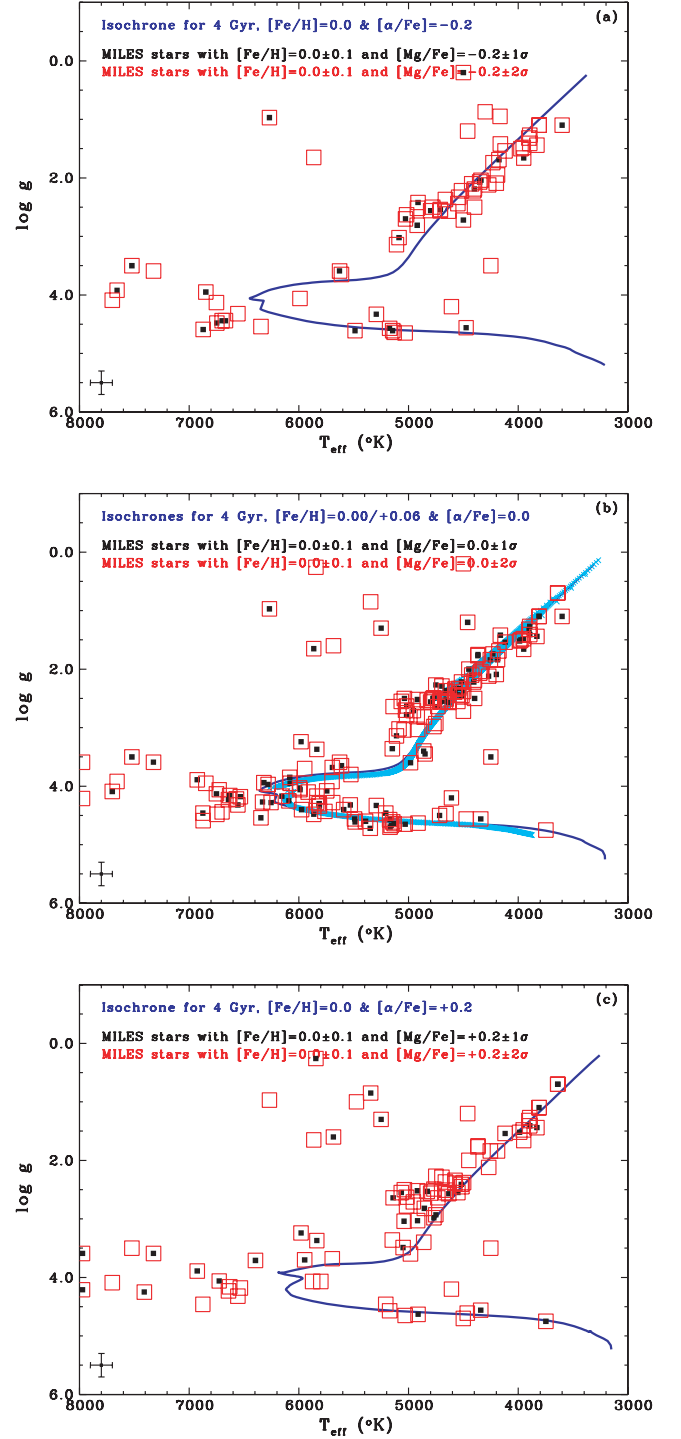

Figure 12. Normalized observed versus normalized model indices for different stars in the MILES library. The normalization of the observations is achieved using MILES stars with the same photospheric parameters as for the models of K05 within errors. These normalizing stars are labelled with 'base' in the plots. The top row shows MILES stars plotted against cool-dwarf star models derived from table 12 of K05; the central row shows MILES stars plotted against turn-off star models derived from table 13 of K05 and the lower row shows MILES stars plotted against cool giant star models derived from table 14 of K05. The models are normalized by the values given in tables 12 to 14 of K05. Models are normalized in the same way as the data, as differences or ratios (see Section 5 for a description). Stars in a given plot all have the same effective temperature and surface gravity as that of the relevant model star, within the errors. The chemistry ([Fe/H] and [α/Fe]) is varied.
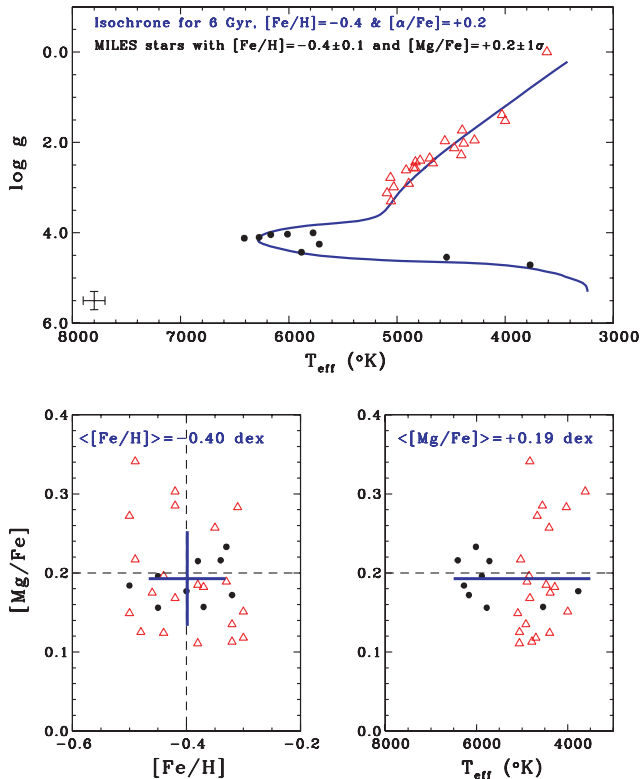
Table 8. Sets of age, metallicity [Fe/H] and [Mg/Fe] (representing α-enhancement) for which there are reasonable number of dwarf and giant stars in MILES to build up semi-empirical SSP models. The star counts are shown for the MS, main sequence turn-off (TO), sub-giants (SG) and red giant branch (RGB) stages. The Dartmouth isochrones (Dotter et al. 2008) have been adopted as reference for this purpose. The stars have been selected in the [Fe/H]-[Mg/Fe] parameter space assuming specified ranges around these quantities, whose criterion of choice was such that the sum of stars in the MS + TO stages ≥ 5 and in the SG + RGB stages ≥ 10. The weighted average σ[Mg/Fe] is 0.105 dex in our catalogue and σ[Fe/H] is 0.10 dex in MILES. Isochrone-based plots for the combinations assigned by asterisks are presented in Figs 13 and 14.

Age (Gyr)	[Fe/H] (dex)	[Mg/Fe] (dex)	MS	TO	SG	RGB
1 ± 2	$+0.4 \pm 0.2$	$-0.2 \pm 2\sigma$	6	7	3	7
1 ± 2	$+0.4 \pm 0.2$	$0.0 \pm 2\sigma$	13	5	3	10
1 ± 2	$+0.5 \pm 0.2$	$0.0 \pm 2\sigma$	8	3	3	7
2 ± 2	0.0 ± 0.1	$-0.2 \pm 1\sigma$	5	4	1	13
2 ± 2	0.0 ± 0.1	$0.0 \pm 1\sigma$	24	9	4	35
2 ± 2	0.0 ± 0.1	$+0.2 \pm 1\sigma$	3	3	3	15
2 ± 2	0.0 ± 0.2	$+0.4 \pm 2\sigma$	3	3	1	13
2 ± 2	$+0.2 \pm 0.1$	$-0.2 \pm 2\sigma$	9	4	2	14
2 ± 2	$+0.2 \pm 0.1$	$0.0 \pm 1\sigma$	12	8	3	15
2 ± 2	$+0.2 \pm 0.1$	$+0.2 \pm 2\sigma$	8	7	4	16
4 ± 2	-0.2 ± 0.1	$-0.2 \pm 2\sigma$	4	4	0	17
4 ± 2	-0.2 ± 0.1	$0.0 \pm 1\sigma$	11	8	1	30
4 ± 2	-0.2 ± 0.1	$+0.2 \pm 1\sigma$	4	7	0	16
4 ± 2	-0.2 ± 0.2	$+0.4 \pm 2\sigma$	5	2	1	22
$*4 \pm 2$	0.0 ± 0.1	$-0.2 \pm 2\sigma$	7	2	3	33
$*4 \pm 2$	0.0 ± 0.1	$0.0 \pm 1\sigma$	19	7	6	44
$*4 \pm 2$	0.0 ± 0.1	$+0.2 \pm 2\sigma$	8	3	4	32
6 ± 2	-0.4 ± 0.1	$0.0 \pm 1\sigma$	3	4	1	9
$*6 \pm 2$	-0.4 ± 0.1	$+0.2 \pm 1\sigma$	4	3	2	21
6 ± 2	-0.4 ± 0.1	$+0.4 \pm 2\sigma$	4	1	2	16
8 ± 2	-0.6 ± 0.2	$0.0 \pm 2\sigma$	4	5	2	14
8 ± 2	-0.6 ± 0.1	$+0.2 \pm 1\sigma$	3	5	2	9
8 ± 2	-0.6 ± 0.1	$+0.4 \pm 1\sigma$	2	4	1	13
10 ± 2	-0.8 ± 0.1	$+0.4 \pm 2\sigma$	4	4	2	14
10 ± 2	-0.6 ± 0.2	$0.0 \pm 2\sigma$	3	4	2	14
10 ± 2	-0.6 ± 0.1	$+0.2 \pm 1\sigma$	3	5	2	9
10 ± 2	-0.6 ± 0.1	$+0.4 \pm 1\sigma$	2	3	2	10
12 ± 2	-2.0 ± 0.2	$+0.4 \pm 2\sigma$	4	2	2	11
12 ± 2	-1.0 ± 0.2	$+0.4 \pm 2\sigma$	5	8	4	20
12 ± 2	-1.0 ± 0.2	$+0.6 \pm 2\sigma$	4	1	1	15
14 ± 1	-2.0 ± 0.2	$+0.4 \pm 2\sigma$	2	7	2	11
14 ± 1	-1.8 ± 0.2	$+0.4 \pm 2\sigma$	3	6	3	11
14 ± 1	-1.6 ± 0.2	$+0.4 \pm 2\sigma$	5	8	4	13
14 ± 1	-1.4 ± 0.1	$+0.2 \pm 2\sigma$	3	2	2	12
14 ± 1	-1.4 ± 0.1	$+0.4 \pm 2\sigma$	4	4	1	13
14 ± 1	-1.2 ± 0.2	$+0.2 \pm 2\sigma$	2	5	1	12

Figure 13. Isochrone-based plots on the HR diagram $\log g$ versus $T_{\rm eff}$ for age 4 Gyr, [Fe/H] = 0.0 dex and three different [α/Fe] (-0.2, 0.0 and $+0.2$ dex), by adopting MILES stars with [Fe/H] = 0.0 dex and [Mg/Fe] around these α-enhancements with 1 and 2 standard deviations (σ): top panel (a) for [Mg/Fe] = -0.2 dex, middle panel (b) for [Mg/Fe] = 0.0 dex, and bottom panel (c) for [Mg/Fe] = $+0.2$ dex. The Dartmouth isochrones (Dotter et al. 2008) are drawn as thick blue lines. In the panel (b), a BaSTI overshooting scaled solar model for [Fe/H] = $+0.06$ dex (Pietrinferni et al. 2006) is also drawn (cyan crosses). The library stars are shown as filled black squares for which [Mg/Fe] has 1σ precision and as open red squares for 2σ.

semi-empirical modelling of a single-age single-metallicity single-α-enhanced stellar population. The isochrone-based plot of this figure on the $\log g$ versus $T_{\rm eff}$ plane is done for 6 Gyr, [Fe/H] = -0.4 dex and [α/Fe] = $+0.2$ dex based on a Dartmouth theoretical model. The MILES stars have been carefully chosen with metallicity and [Mg/Fe] around the isochrone values within 1σ. Furthermore, the restrictive matching of the stars' positions with the isochrone

Figure 14. Example of a cross-matching between a selected group of MILES stars and an isochrone for SSP modelling. Top panel: isochrone-based plot on the H-R diagram log g versus T_{eff} for 6 Gyr, [Fe/H] = −0.4 dex and [α/Fe] = +0.2 dex by collecting MILES stars with metallicity and [Mg/Fe] around these values with 1σ deviation that restrictively match the correspondent Dartmouth isochrone (Dotter et al. 2008) taking into account the MILES errors in log g and T_{eff} within 1σ too (error bars placed in the bottom left corner). The dwarfs are represented as black filled circles and giants as red open triangles in all plots, where dwarfs have log $g \geq 3.7$, covering the stages MS, TO and SG listed in Table 8, and giants log $g < 3.7$. Bottom-left panel: [Mg/Fe] versus [Fe/H] plot for the selected dwarfs and giants, in which the two blue thick lines show the stars' average values of [Fe/H] and [Mg/Fe] (the line lengths are equal to the standard deviations of the averages). Bottom-right panel: [Mg/Fe] versus T_{eff} plot for the selected dwarfs and giants, in which the horizontal blue thick line shows the stars' average [Mg/Fe] over the whole stellar sample temperature scale. The averages of [Fe/H] and [Mg/Fe] are written on the top of left- and right-hand panels, respectively.

has considered the MILES errors in log g and T_{eff} within 1σ too. We have also computed the averages of [Fe/H] and [Mg/Fe] for the selected stars to check if there is agreement with the model's values. In this cross-matching SSP-MILES, nine dwarfs (log $g \geq 3.7$) and 21 giants have been selected whose averages [Fe/H] and [Mg/Fe] are −0.40 and +0.19 dex, respectively, in excellent accordance with the SSP's parameters (the standard deviations are σ[Fe/H] = 0.07 dex and σ[Mg/Fe] = 0.06 dex). The stars are roughly well sampled along the isochrone although there are some empty places that might be filled through interpolations applied in the library parameter space. This procedure must make the stars' distribution more uniform around the model chemistry shown, for instance, in the plane [Fe/H] versus [Mg/Fe], refining in this way the computation of the SSP observables.

We have also begun a study of the dependence of absorption line indices on [Mg/Fe], focusing on the observed behaviour of some indices of the Lick System as a function of the photospheric

parameters, as described in Section 5. We intend to compute semi-empirical fitting functions for the main Lick indices in order to improve and extend the SSP models for different α-enhancements.

The predictions of new semi-empirical SSP models will be compared with the observables of distinct composite stellar systems such as globular clusters, dwarf galaxies, ellipticals and spiral bulges. Consequently, the models will be very useful to understand their star formation histories and chemical evolutions.

Moreover, we can test and apply the same approach of this work to obtaining the calcium abundances for the MILES stars. Indeed, there are interesting questions about how the calcium-enhancement behaves in several composite stellar systems relative to other α-elements like magnesium. For instance, Smith et al. (2009b) found for a sample of 147 red-sequence galaxies from the Coma cluster and the Shapley Supercluster that the [Ca/Fe] ratio is positively correlated with the velocity dispersion, at fixed [Fe/H], however its dependence is significantly less steep than that of [Mg/Fe]. On the other hand, Pipino et al. (2009a) obtained that the [Ca/Fe]–mass relation is naturally explained by such a standard galactic chemical evolution model, and explained that the observed underabundance of Ca with respect to Mg can be attributed to the different contributions from Type Ia and Type II supernovae to the nucleosynthesis of these two elements.

Additional applications of the present [Mg/Fe] catalogue will potentially improve areas of our understanding of stellar atmospheres and spectral flux distributions from different types of stars present in the MILES library.

7 CONCLUSIONS AND SUMMARY

We have obtained [Mg/Fe] for 76.3 per cent of the MILES stellar library (411 dwarfs and 341 giants, 76 per cent and 77 per cent of the total, respectively), suitable for SSP modelling. The weighted average uncertainty σ[Mg/Fe] is 0.105 dex over this MILES [Mg/Fe] catalogue.

The compilation of high spectral resolution [Mg/Fe] abundance ratios in the literature was extremely useful in defining a uniform scale for [Mg/Fe] and in obtaining an extensive reference sample for the calibration of abundance ratios measured in our work at medium resolution. We emphasize that the calibration of MR measurements is an important step to be done in the whole process to achieve reliable results in a homogeneous reference system.

A robust spectroscopic analysis was carried out using the MILES MR spectra and LTE spectral synthesis of two Mg features. Two methods were applied through an automatic process: pseudo-equivalent width and LPF.

The typical error of [Mg/Fe] from the collected and calibrated HR measurements is 0.09 dex, and the uncertainties from our MR analysis range from 0.10 to 0.15 dex, with a weighted average of 0.12 dex. Thus, we show that the accuracy of our measurements from MR spectra is quite acceptable, but not better than those from HR analyses. It is possible to measure element abundances in many more stars with such accuracy at MR when a large control sample from HR measurements is adopted. Hence, this catalogue of [Mg/Fe] measurements will be useful for a range of applications for stellar population modelling and understanding stellar spectra.

The pattern of [Mg/Fe] versus [Fe/H] found for the stars in the MILES library is as expected for stars in the solar neighbourhood, ranging from sub-solar [Mg/Fe] for high-metallicity stars to super-solar [Mg/Fe] for low-metallicity stars, as shown in Fig. 10.

[Mg/Fe] measurements approximately characterize the alpha-to-iron ratios in stars. Although not all types of stellar populations

would be well sampled by the stars in this catalogue, applications exploring the effects of non-solar abundance ratios will be possible for such objects as globular clusters, spiral galaxies, various types of low-luminosity galaxies and dwarf galaxies. The importance of this is: (i) abundance patterns in stellar populations hold clues to their histories and (ii) the accuracies of previously used characterizations of abundance patterns, based on theoretical models, can now be tested. These applications will be followed up in future work.

We also plan to use the MILES [Mg/Fe] catalogue to compute empirical and self-consistent models of stellar populations with Mg/Fe different from solar for certain values of age and metallicity. These models will serve as a benchmark for other models based on theoretical libraries as they will allow calibration of the effects of uncertainties in the final predictions due to uncertainties in specific groups of stars. We will study empirically the dependences of Lick System indices as a function of the Mg/Fe ratio by adopting MILES stars with similar photospheric parameters but showing distinct [Mg/Fe] in order to help computing robust stellar fitting functions of line strengths. Comparisons of empirical and theoretical line strengths will also be made (Sansom et al., in preparation).

REFERENCES

Adelman S. J., Caliskan H., Kocer D., Kablan H., Yüce K., Engin S., 2001, A&A, 371, 1078 (Ae01)
Adelman S. J., Caliskan H., Gulliver A. F., Teker A., 2006, A&A, 447, 685 (Ae06)
Bensby T., Feltzing S., Lundström I., Ilyin I., 2005, A&A, 433, 185 (Be05)
Bensby T., Alves-Brito A., Oey M. S., Yong D., Meléndez J., 2010, A&A, 516, L13
Bertone E., Buzzoni A., Chávez M., Rodríguez-Merino L. H., 2008, A&A, 485, 823
Borkova T. V., Marsakov V. A., 2005, AZh, 82, 453 (BM05)
Caliskan H., Adelman S. J., Cay M. T., Cay I. H., Gulliver A. F., Tektunali G. H., Kocer D., Teker A., 2002, A&A, 394, 187 (Ce02)
Cardiel N., Gorgas J., Cenarro J., Gonzalez J. J., 1998, A&AS, 127, 597
Carretta E., Gratton R. G., Sneden C., 2000, A&A, 356, 238 (CGS00)
Cenarro A. J., Gorgas J., Cardiel N., Pedraz S., Peletier R. F., Vazdekis A., 2001, MNRAS, 326, 981
Cenarro A. J., Gorgas J., Cardiel N., Vazdekis A., Peletier R. F., 2002, MNRAS, 329, 863
Cenarro A. J. et al., 2007, MNRAS, 374, 664
Cenarro A. J., Cardiel N., Vazdekis A., Gorgas J., 2009, MNRAS, 396, 1895
Chavez M., Malagnini M. L., Morossi C., 1995, ApJ, 440, 210
Chavez M., Malagnini M. L., Morossi C., 1997, A&AS, 126, 267

Chen Y. Q., Nissen P. E., Zhao G., Zhang H. W., Benoni T., 2000, A&AS, 141, 491
Coelho P., Barbuy B., Meléndez J., Schiavon R. P., Castilho B. V., 2005, A&A, 443, 735
Coelho P., Bruzual G., Charlot S., Weiss A., Barbuy B., Ferguson J. W., 2007, MNRAS, 382, 498
Cohen J. G., Meléndez J., 2005, AJ, 129, 303 (CM05)
Cook D., Shetrone M., Siegel M., Bosler T., 2007, A&AS, 211, 9513
Denicoló G., Terlevich R., Terlevich E., Forbes D. A., Terlevich A., 2005, MNRAS, 358, 813
Dotter A., Chaboyer B., Jevremović D., Kostov V., Baron E., Ferguson J. W., 2008, ApJS, 178, 89
Erspamer D., North P., 2003, A&A, 398, 112 (EN03)
Feltzing S., Gustafsson B., 1998, A&AS, 129, 237 (FG98)
Fiorentin P., Bailer-Jones C. A. L., Lee Y. S., Beers T. C., Sivarani T., Wilhelm R., Allende Prieto C., Norris J. E., 2007, A&A, 467, 1373
Frémaux J., Kupka F., Boisson C., Joly M., Tsymbal V., 2006, A&A, 449, 109
Friel E. D., Janes K. A., 1993, A&A, 267, 75
Friel E. D., Janes K. A., Tavarez M., Scott J., Katsanis R., Lotz J., Hong L, Miller N., 2002, AJ, 124, 2693
Fulbright J. P., 2000, AJ, 120, 1841 (F00)
Fulbright J. P., Kraft R. P., 1999, AJ, 118, 527 (FK99)
Gebran M., Monier R., Richard O., 2008, A&A, 479, 189 (GMR08)
Gratton R. G., Ortolani S., 1989, A&A, 211, 41
Gratton R. G., Carretta E., Claudi R., Lucatello S., Barbieri M., 2003, A&A, 404, 187 (Ge03)
Grevesse N., Asplund M., Sauval A. J., 2007, Space Sci. Rev., 130, 205 (GAS07)
Gustafsson B., Edvardsson B., Eriksson K., Jörgensen U. G., Nordlund Å., Plez B., 2008, A&A 486, 951
Heiter U., 2002, A&A, 381, 959 (H02)
Ivans I. I., Sneden C., James C. R., Preston G. W., Fulbright J. P., Höflich P. A., Carney B. W., Wheeler J. C., 2003, ApJ, 592, 906
Johnson C. I., Kraft R. P., Pilachowski C. A., Sneden C., Ivans I. I., Benman G., 2005, PASP, 117, 1308 (Je05)
King J. R., Soderblom D. R., Fischer D., Jones B. F., 2000, ApJ, 533, 944 (Ke00)
Kirby E. N., Guhathakurta P., Bolte M., Sneden C., Geha M. C., 2009, ApJ, 705, 328
Korn A. J., Maraston C., Thomas D., 2005, A&A, 438, 685 (K05)
Kupka F., Piskunov N. E., Ryabchikova T. A., Stempels H. C., Weiss W. W., 1999, A&AS, 138, 119
Kupka F., Ryabchikova T. A., Piskunov N. E., Stempels H. C., Weiss W. W., 2000, Baltic Astron., 9, 590
Kurucz R., 1995, in Sauval A. J., Blomme R., Grevesse N., eds, ASP Conf. Ser. Vol. 81, Laboratory and Astronomical High Resolution Spectra. Astron. Soc. Pac., San Francisco, p. 583
Lee H.-C., Worthey G., 2005, ApJS, 160, 176
Lee H.-C., Worthey G., Dotter A., 2009, ApJ, 694, 902
Luck R. E., Heiter U., 2005, AJ, 129, 1063 (LH05)
Marsteller B., Beers T. C., Thirupathi S., Rossi S., Placco V., Knapp G. R., Johnson J. A., Lucatello S., 2009, AJ, 138, 533
Martins L. P., Coelho P., 2007, MNRAS, 381, 1329
Martins L. P., González Delgado R. M., Leitherer C., Cerviō M., Hauschildt P., 2005, MNRAS, 358, 49
Masseron T., 2008, PhD thesis, Ohio State Univ.
Meléndez J., Cohen J. G., 2009, ApJ, 699, 2017 (MC09)
Mishenina T. V., Soubiran C., Kovtyukh V. V., Korotin S. A., 2004, A&A, 418, 551
Munari U., Sordo R., Castelli F., Zwitter T., 2005, A&A, 442, 1127
Murphy T., Meiksin A., 2004, MNRAS, 351, 1430
Neves V., Santos N. C., Sousa S. G., Correia A. C. M., Israelian G., 2009, A&A, 497, 563
Nissen P. E., Schuster W. J., 2010, A&A, 511, 10
Pagel B. E. J., 1970, Vistas Astron., 12-1, 313
Pancino E., Carrera R., Rossetti E., Gallart C., 2010, A&A, 511, 56 (Pe10)
Paulson D. B., Sneden C., Cochran W. D., 2003, AJ, 125, 3185 (PSC03)

Pietrinferni A., Cassisi S., Salaris M., Castelli F., 2004, ApJ, 612, 168

Pietrinferni A., Cassisi S., Salaris M., Castelli F., 2006, ApJ, 642, 797

Pilachowski A. A., 1985, PASP, 97, 801

Pipino A., Chiappini C., Graves G., Matteucci F., 2009a, MNRAS, 396, 1151

Pipino A., Devriendt J. E. G., Thomas D., Silk J., Kaviraj S., 2009b, A&A, 505, 1075

Piskunov N. E., Kupka F., Ryabchikova T. A., Weiss W. W., Jeffery C. S., 1995, A&AS, 112, 525

Proctor R. N., Sansom A. E., 2002, MNRAS, 333, 517

Ramírez S. V., Cohen J. G., 2002, AJ, 123, 3277 (RC02)

Reddy B. E., Lambert D. L., Allende Prieto C., 2006, MNRAS, 367, 1329 (RLA06)

Rodriguez-Merino L. H., Chavez M., Bertone E., Buzzoni A., 2005, ApJ, 626, 411

Ryabchikova T. A., Piskunov N. E., Kupka F., Weiss W. W., 1997, Baltic Astron., 6, 244

Sánchez-Blázquez P. et al., 2006, MNRAS, 371, 703

Schiavon R. P., 2007, ApJS, 171, 146

Schuler S. C., King J. R., Lih-Sin, 2009, ApJ, 701, 837 (SKL09)

Serven J., Worthey G., Briley M. M., 2005, ApJ, 627, 754

Shetrone M. D., 1996, AJ, 112, 1517

Smith R. J., Lucey J. R., Hudson M. J., 2009a, MNRAS, 400, 1690

Smith R. J., Lucey J. R., Hudson M. J., Bridges T. J., 2009b, MNRAS, 398, 119

Sneden C., 2002, The MOOG code, http://verdi.as.utexas.edu/moog.html

Sneden C., Kraft R. P., Guhathakurta P., Peterson R. C., Fulbright J. P., 2004, AJ, 127, 2162 (Se04)

Stephens A., Ann Merchant B., 2002, AJ, 123, 1647

Tantalo R., Chiosi C., Bressan A., 1998, A&A, 333, 419

Terndrup D. M., Sadler E. M., Rich R. M., 1995, AJ, 110, 1774

Thévenin F., 1998, VizieR On-line Data Catalog: III/193

Thomass D., Maraston C., Bender R., 2003, MNRAS, 339, 897

Tinsley B. M., 1980, Fundam. Cosmic Phys., 5, 287

Trager S. C., Faber S. M., Worthey G., González J. J., 2000a, AJ, 119, 1645

Trager S. C., Faber S. M., Worthey G., González J. J., 2000b, AJ, 120, 165

Tripicco M. J., Bell R. A., 1995, AJ, 110, 3035

Vazdekis A., Peletier R. F., Beckman J. E., 1997, ApJS, 111, 203

Vazdekis A., Sánchez-Blázquez P., Falcón-Barroso J., Cenarro A. J., Beasley M. A., Cardiel N., Gorgas J., Peletier R. F., 2010, MNRAS, 404, 1639

Walcher C. J., Coelho P., Gallazzi A., Charlot S., 2009, MNRAS, 398, L44

Weiss A., Peletier R. F., Matteucci F., 1995, A&A, 296, 73

Yong D., Lambert D. L., Allende Prieto C., 2004, ApJ, 603, 697 (YLA04)

APPENDIX A: COMPARISON WITH CENARRO ET AL. (2009)

This appendix shows the comparison of our [Mg/Fe] reference scale with the CaT catalogue (Cenarro et al. 2009).

Fig. A1 presents a direct comparison of the [Mg/Fe] HR measurement compilation done by Cenarro et al. (2009) for their CaT library stars with the HR part of MILES [Mg/Fe] catalogue. A linear LSQ fitting between their results and ours (also considering the errors in both variables and minimizing the distance along both directions) gives $[Mg/Fe]_{CaT} = [Mg/Fe]_{Ce09} = 0.00 + 0.95 [Mg/Fe]_{MILES}$ with a data spreading of 0.03 dex (*rms*). This fit shows deviations, which are 0.035 dex at maximum, comfortably within the correspondent uncertainties of [Mg/Fe] in CaT (typically 0.14 dex) and MILES (0.09 dex on average). Two pairs of data were excluded by the 3σ clipping treatment taking into account their errors as well. Few outliers with high and low [Mg/Fe] values (all from T98) were also excluded from this comparison. The *t*-test with a 95 per cent confidence level indicates that the relationship $[Mg/Fe]_{MILES}$ versus $[Mg/Fe]_{Ce09}$ is not far from the 1:1 relation (see Fig. A1). Therefore, there is a quite good agreement between both scales.
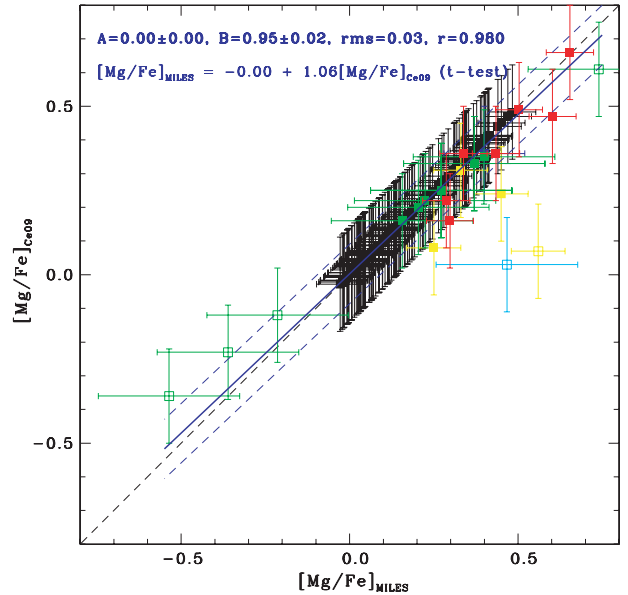

Figure A1. Comparison of our HR data with the [Mg/Fe] compilation for the CaT library (Cenarro et al. 2009) that both have been independently calibrated to that scale of BM05 (whose measurements are represented by the filled black squares). The filled colour squares represent different data sets: blue for CGS00, green for T98, yellow for F00 and red for the stars with duplicated sources. The linear LSQ fit $[Fe/H]_{Cen09} = A + B [Fe/H]_{MILES}$ (solid blue line) is shown with parallel dashed blue lines illustrating the 3σ data clipping (its A and B, *rms* and correlation coefficient r are presented). The statistically representative inverse expression $[Fe/H]_{MILES} = -A/B + 1/B [Fe/H]_{Ce09}$, based on a 95 per cent *t*-test, is also shown on the top. The excluded data are represented by open colour squares (3σ criterion and outliers from T98).

APPENDIX B: COMPARISON OF ATMOSPHERIC PARAMETERS

In this appendix, we investigate possible systematic differences between the atmospheric parameters of the MILES catalogue (Cenarro et al. 2007), that have been adopted all over in the current work, and those of the BM05 sample. Just concerning the metallicity scale, comparisons are also made with the data of those consulted HR works (see Section 2).

Fig. B1-(a)-(l) presents [Fe/H] from 12 consulted works compared with the MILES [Fe/H] scale. Lines of LSQ linear fittings $[Fe/H]_{work} = A + B [Fe/H]_{MILES}$ are shown in these plots. The adopted LSQ method takes into account the errors in both variables by minimizing the sum of distances of all points to the line. Statistically representative inverse linear transformation expressions $[Fe/H]_{MILES} = -A/B + 1/B [Fe/H]_{work}$ are obtained after applying a 95 per cent confidence level *t*-test for each fit parameter ($A \neq 0$? and/or $B \neq 1$?). The fitted straight lines found are very close to the 1:1 relationship. There are tiny systematic differences between the MILES [Fe/H] scale and the scales from Fulbright (2000), Bensby et al. (2005) and Luck & Heiter (2005). However, these differences are dominated by a few outliers, as can be seen in panels (c), (e) and (h), that are specifically localized either at the metal-poor regime on the comparison with the Fulbright (2000) data or over metal-rich stars on the comparisons with the samples of Bensby et al. (2005) and Luck & Heiter (2005). If we applied metallicity corrections for these samples, they would be smaller than the involved uncertainties, even for the works of Bensby et al. (2005), and Luck & Heiter (2005). Therefore, no correction has been applied to the
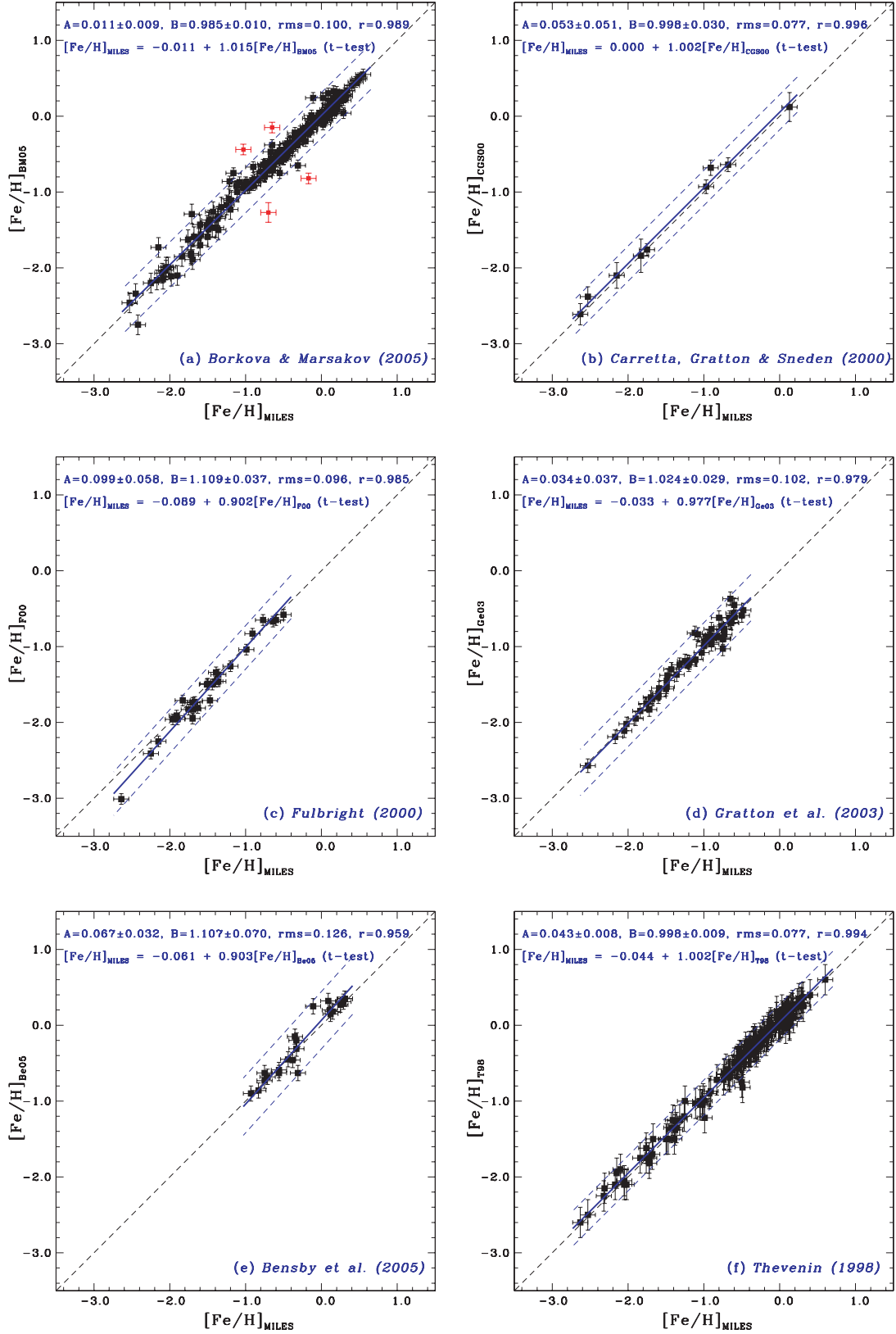
Figure B1. [Fe/H]$_\text{work}$ versus [Fe/H]$_\text{MILES}$: 12 panels (from a to l) showing comparisons between the metallicity scales of the consulted HR works (designation at the bottom of each panel) with the MILES one. The linear LSQ fittings [Fe/H]$_\text{work} = A + B$ [Fe/H]$_\text{MILES}$ with a 3σ data clipping are presented and illustrated by, respectively, solid blue line plus parallel dashed blue lines with excluded points in red. The constants A and B, *rms* and correlation coefficient r are shown on top of each plot as well as the statistically representative inverse expressions [Fe/H]$_\text{MILES} = -A/B + 1/B$ [Fe/H]$_\text{work}$, based on 95 per cent *t*-tests.
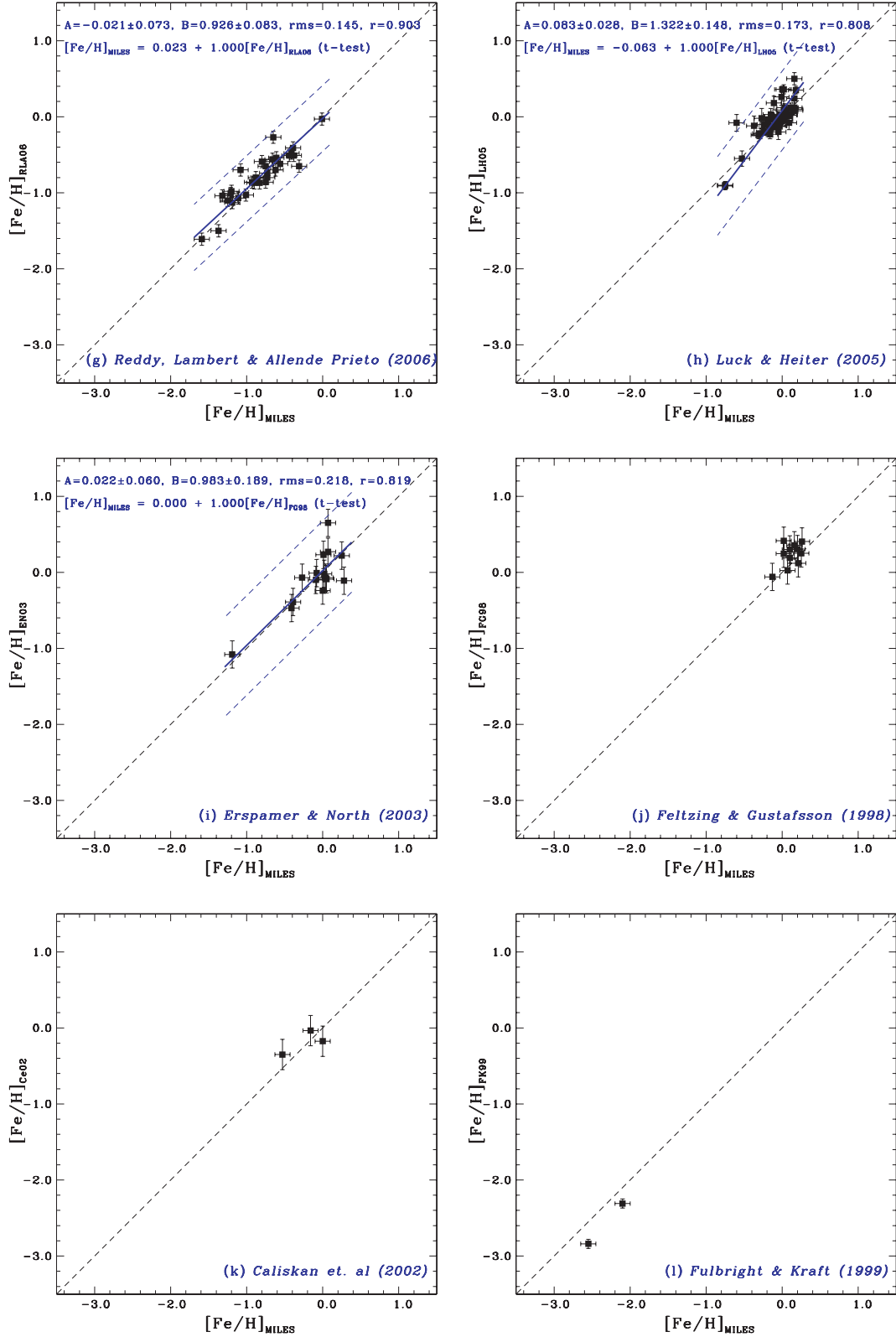
Figure B1 – *continued*

[Fe/H] from the consulted works because no significant systematic deviations from the MILES [Fe/H] scale have been detected.

For the comparison of BM05 and MILES $T_{\rm eff}$ scales, the *rms* of 83 K for a linear relationship between the scales and the respec- tive systematic deviation is comparable to the typical temperature uncertainty in MILES ($1\sigma = 100$ K). In the range 4500–7000 K, for instance, the maximum absolute difference reaches around 55 K only. For the BM05-MILES log g scale comparison, the absolute

Table C1. Averages values of [Mg/Fe] for star clusters in the MILES library computed from two or more star individual measurements at MR done in this work, $\overline{[Mg/Fe]}_{mr}$ and standard deviation $\sigma\overline{[Mg/Fe]}_{mr}$, and respective average from the HR studies, $\overline{[Mg/Fe]}_{HR}$ and standard deviation $\sigma\overline{[Mg/Fe]}_{HR}$. The number of stars for each average (mr and HR) is informed in the columns six and 10, respectively. The clusters' metallicities adopted in MILES are listed in the third column. The Mg features adopted in our MR measurements are presented in the seventh column and the references consulted for the HR data are given in the last column (GMR08 for Gebran, Monier & Richard 2008, SKL09 for Schuler et al. 2009, YLA04 for Yong et al. 2004, PSC03 for Paulson et al. 2003, T98 for Thévenin 1998, Ke00 for King et al. 2000, CM05 for Cohen & Meléndez 2005, Je05 for Johnson et al. 2005, Se04 for Sneden et al. 2004, S96 for Shetrone 1996, MC09 for Meléndez & Cohen 2009, RC02 for Ramírez & Cohen 2002, GO89 for Gratton & Ortolani 1989 and Pe10 for Pancino et al. 2010, on the order they appear in the table). The HR data from T98 (Hyades) come directly from the MILES [Mg/Fe] catalogue. Note: the other $\overline{[Mg/Fe]}_{HR}$ are not transformed on to the catalogue's uniform scale.

Cluster	Type	[Fe/H] (dex)	$\overline{[Mg/Fe]}_{mr}$ (dex)	$\sigma\overline{[Mg/Fe]}_{mr}$ (dex)	N_{mr}	Mg feature(s)	$\overline{[Mg/Fe]}_{HR}$ (dex)	$\sigma\overline{[Mg/Fe]}_{HR}$ (dex)	N_{HR}	Ref.
Coma Ber	Open	−0.05	+0.304	0.022	2	Mg5528	+0.26	0.008	2	GMR08
Hyades	Open	+0.13	−0.035	0.169	10	Both	−0.03	0.02	3	SKL09
							−0.09	0.10	34	YLA04
							−0.03	0.04	55	PSC03
							−0.016	0.063	3	T98
Pleiades	Open	−0.03	−0.122	0.083	2	Both	−0.01	0.06	2	Ke00
M3	Globular	−1.34	+0.299	0.183	3	Both	+0.41	0.12	13	CM05
							+0.17	0.15	77	Je05
							+0.22	0.15	23	Se04
M5	Globular	−1.11	+0.426	0.169	2	Both	+0.16	0.07	6	S96
M71	Globular	−0.84	+0.485	0.104	19	Both	+0.20	0.10	9	MC09
							+0.36	0.09	24	RC02
							+0.34	0.08	8	S96
M79	Globular	−1.37	+0.493	0.009	2	Mg5528	+0.47	0.45	2	GO89
M92	Globular	−2.16	+0.485	0.173	2	Mg5528	+0.19	0.19	6	S96
NGC 7789	Open	−0.13	+0.077	0.092	13	Both	+0.22	0.10	3	Pe10

difference in the interval 3.0–5.0 gets a maximum of 0.13, which is smaller than the MILES log g uncertainty ($1\sigma = 0.20$). The *rms* of the linear relationship between the gravity scales is smaller than the gravity's uncertainty too (0.145). The angular coefficients of the linear LSQ fits T_{eff}(BM05) versus T_{eff}(MILES) and log g(BM05) versus log g(MILES) are different, respectively, 1 per cent and 11 per cent only from that of the 1:1 relation. Therefore, the scales of T_{eff} and log g in BM05 and MILES agree quite well between each other, and no correction has been applied to these stellar parameters too.

APPENDIX C: COMPARISONS OF STAR CLUSTER DATA

In this appendix, comparisons with stars cluster data from HR studies are presented.

There are 89 cluster stars in the MILES data base (from nine open clusters and eight globular clusters). Our MR measurements cover 65 cluster members (73 per cent of them) including 16 out of 17 clusters of MILES (see Table 5, Section 4). Specifically for three star clusters presented in MILES (Hyades, M71 and NGC7789), we have obtained [Mg/Fe] for a reasonable number of members from our spectral synthesis at MR (≥ 10 stars). Average values are presented in Table C1 together with the results from other clusters for which we have done MR measurements for a minimum of two stars, providing an interesting quality test for our work. The table also shows average cluster values of [Mg/Fe] collected from HR studies, but their abundance ratios are not in the same uniform scale adopted in the current work. The literature cluster averages [Mg/Fe] are computed from published ratios to be representative to the star sample analysed in our work for each cluster in terms of spectral type and luminosity class.

For the open cluster Hyades only ([Fe/H] = +0.13 dex), we could compare our [Mg/Fe] MR measurements directly with the compiled HR data in a same uniform scale. The average [Mg/Fe] computed from the MR measurements based on the two Mg features and including 10 members (dwarfs only with $5256 \leq T_{eff} \leq 7634$ K) is −0.035 dex with a standard deviation $\sigma = 0.169$ dex, whilst the HR data have an average value −0.016 ($1\sigma = 0.063$ dex) from three dwarfs only (all from T98 with $T_{eff} = 6486$, 6742 and 8850 K). The average of [Mg/Fe] from both MR and HR data for Hyades is −0.030 ($\sigma = 0.149$ dex). Schuler, King & Lih-Sin (2009) have recently measured, by analysing high-S/N HR spectra, [Mg/H] = +0.10 ($\sigma = 0.02$ dex) in three MS stars (T_{eff} around 5600 K), getting [Mg/Fe] = −0.03 dex. A sample of 55 *F-K* dwarfs (with $4900 \leq T_{eff} \leq 6450$ K) was spectroscopically analysed at HR and high S/N by Paulson, Sneden & Cochran (2003). They obtained [Fe/H] = +0.13 ± 0.01 dex and differentially [Mg/Fe] = −0.03 ± 0.04 dex. The spectroscopic analysis (based on HR and high-S/N spectra) of Yong, Lambert & Allende Prieto (2004) measures for 34 Hyades dwarfs with $4700 < T_{eff} \leq 6200$ K cluster averages of [Fe/H] = −0.16 ($\sigma = 0.10$ dex) and [Mg/Fe] $\approx$ −0.09 dex. All these results corroborate our work.

For the globular cluster M71 ([Fe/H] = −0.84 dex), in which there is a known internal spread of α/Fe ratio over the stars (Ramírez & Cohen 2002), we obtained an average [Mg/Fe] abundance ratio equal to +0.485 ($\sigma = 0.104$ dex) based on measurements from both Mg features in 19 cluster members, which are all giants with $4014 \leq T_{eff} \leq 5123$ K. [Mg/Fe] varies in M71 as Ramírez & Cohen (2002) measured in 24 giants that were spectroscopically analysed at HR. This star sample exhibits an average [Mg/Fe] equal to +0.36 ($\sigma = 0.09$ dex) and a maximum internal spread of 0.18 dex. Meléndez & Cohen (2009) recently proved, as concluded in other previous studies, the existence of two stellar populations in M71; one CN-weak with normal O, Na, Mg and Al abundances plus a low isotope

abundance ratio of ^{26}Mg/^{24}Mg, and other CN-strong with enhanced Na and Al accompanied by lower O together with a higher ratio ^{26}Mg/^{24}Mg. However, they measured a small spread for [Mg/Fe] over nine giants (0.10 dex at most) belonged to both internal populations exhibiting an average around +0.20 dex.

For the galactic cluster NGC 7789 ([Fe/H] = −0.13 dex), the average [Mg/Fe] is +0.077 (σ = 0.092 dex) from our Mg5183/Mg5528 measurements in 13 giant stars (with 4020 ≤ T_{eff} ≤ 4952 K). A very recent work (Pancino et al. 2010) has measured for it an average [Fe/H] = +0.04 ± 0.07 with 1σ dispersion of 0.10 dex and [Mg/Fe] = +0.22 ± 0.07 (σ = 0.10 dex) based on spectroscopic measurements of three red clump stars with high-quality spectra at HR, whilst previous studies at lower spectral resolution and through photometry-based techniques obtained [Fe/H] ≃ −0.2 dex with [X/Fe] around zero for many elements (e.g. Pilachowski 1985; Friel et al. 2002).

Concerning our star cluster data, the major conclusions are: (i) the standard deviations of computed average cluster values of [Mg/Fe] are comparable with the systematic uncertainties of our individual MR measurements as well as with the dispersion of the cluster average abundance ratios collected from the HR studies, and (ii) the [Mg/Fe] averages from the current work are in good agreement with measurements carried out with high-S/N HR spectra in recent studies.

SUPPORTING INFORMATION

Additional Supporting Information may be found in the online version of this article:

Table 4. The MILES [Mg/Fe] catalogue for field stars.
Table 5. The MILES [Mg/Fe] catalogue for star cluster stars (as in Table 4).

Please note: Wiley-Blackwell are not responsible for the content or functionality of any supporting materials supplied by the authors. Any queries (other than missing material) should be directed to the corresponding author for the article.

This paper has been typeset from a TEX/LATEX file prepared by the author.